AFRL-PR-WP-TR-2004-2128

VOLUME AND SURFACE PLASMAS

Biswa N. Ganguly

Plasma Physics Branch (AFRL/PRPE)
Power Division
Propulsion Directorate
Air Force Materiel Command, Air Force Research Laboratory
Wright-Patterson Air Force Base, OH 45433-7251

SEPTEMBER 2004

Final Report for 01 February 1989 – 01 September 2004

STINFO FINAL REPORT

PROPULSION DIRECTORATE
AIR FORCE MATERIEL COMMAND
AIR FORCE RESEARCH LABORATORY
WRIGHT-PATTERSON AIR FORCE BASE, OH 45433-7251

NOTICE

USING GOVERNMENT DRAWINGS, SPECIFICATIONS, OR OTHER DATA INCLUDED IN THIS DOCUMENT FOR ANY PURPOSE OTHER THAN GOVERNMENT PROCUREMENT DOES NOT IN ANY WAY OBLIGATE THE U.S. GOVERNMENT. THE FACT THAT THE GOVERNMENT FORMULATED OR SUPPLIED THE DRAWINGS, SPECIFICATIONS, OR OTHER DATA DOES NOT LICENSE THE HOLDER OR ANY OTHER PERSON OR CORPORATION; OR CONVEY ANY RIGHTS OR PERMISSION TO MANUFACTURE, USE, OR SELL ANY PATENTED INVENTION THAT MAY RELATE TO THEM.

THIS REPORT HAS BEEN REVIEWED BY THE AIR FORCE RESEARCH LABORATORY WRIGHT SITE OFFICE OF PUBLIC AFFAIRS (AFRL/WS/PA) AND IS RELEASABLE TO THE NATIONAL TECHNICAL INFORMATION SERVICE (NTIS). AT NTIS, IT WILL BE AVAILABLE TO THE GENERAL PUBLIC, INCLUDING FOREIGN NATIONALS.

THIS TECHNICAL REPORT HAS BEEN REVIEWED AND IS APPROVED FOR PUBLICATION.

/s/

BISWA N. GANGULY
Principal Research Physicist
Plasma Physics Branch

/s/

ROBERT H. LEE
Acting Branch Chief
Plasma Physics Branch

/s/

CYNTHIA A. OBRINGER
Deputy Chief
Power Division

IF YOUR ADDRESS HAD CHANGED, IF YOU WISH TO BE REMOVED FROM OUR MAILING LIST, OR IF THE ADDRESSEE IS NO LONGER EMPLOYED BY YOUR ORGANIZATION, PLEASE NOTIFY AFRL/PRPE, WRIGHT-PATTERSON AFB, OH 45433-7251 TO HELP MAINTAIN A CURRENT MAILING LIST.

COPIES OF THIS REPORT SHOULD NOT BE RETURNED UNLESS RETURN IS REQUIRED BY SECURITY CONSIDERATIONS, CONTRACTUAL OBLIGATIONS, OR NOTICE ON A SPECIFIC DOCUMENT.

REPORT DOCUMENTATION PAGE

Form Approved
OMB No. 0704-0188

1. REPORT DATE *(DD-MM-YY)*	2. REPORT TYPE	3. DATES COVERED *(From - To)*
September 2004	Final	02/01/1989 – 09/01/2004

4. TITLE AND SUBTITLE
VOLUME AND SURFACE PLASMAS

5a. CONTRACT NUMBER
In-House

5b. GRANT NUMBER

5c. PROGRAM ELEMENT NUMBER
61102F

6. AUTHOR(S)
Biswa N. Ganguly

5d. PROJECT NUMBER
2301

5e. TASK NUMBER
S1

5f. WORK UNIT NUMBER
10

7. PERFORMING ORGANIZATION NAME(S) AND ADDRESS(ES)

Plasma Physics Branch (AFRL/PRPE)
Power Division
Propulsion Directorate
Air Force Materiel Command, Air Force Research Laboratory
Wright-Patterson Air Force Base, OH 45433-7251

8. PERFORMING ORGANIZATION REPORT NUMBER
AFRL-PR-WP-TR-2004-2128

9. SPONSORING/MONITORING AGENCY NAME(S) AND ADDRESS(ES)

Propulsion Directorate
Air Force Research Laboratory
Air Force Materiel Command
Wright-Patterson AFB, OH 45433-7251

10. SPONSORING/MONITORING AGENCY ACRONYM(S)
AFRL/PRPE

11. SPONSORING/MONITORING AGENCY REPORT NUMBER(S)
AFRL-PR-WP-TR-2004-2128

12. DISTRIBUTION/AVAILABILITY STATEMENT
Approved for public release; distribution is unlimited.

13. SUPPLEMENTARY NOTES
Report contains color.

14. ABSTRACT

Scaling of volume and surface dominated plasmas were quantified by electrical, microwave and optical measurements. The application of these plasma devices range from RF plasma processing, high flux atom production, plasma switch and plasma assisted combustion.

15. SUBJECT TERMS
plasmas, laser spectroscopy of atoms and molecules, wide bandgap semiconductor, etching, double layer plasma

16. SECURITY CLASSIFICATION OF:			17. LIMITATION OF ABSTRACT:	18. NUMBER OF PAGES	19a. NAME OF RESPONSIBLE PERSON (Monitor)
a. REPORT	b. ABSTRACT	c. THIS PAGE			Biswa N. Ganguly
Unclassified	Unclassified	Unclassified	SAR	64	19b. TELEPHONE NUMBER *(Include Area Code)* (937) 255-2923

Standard Form 298 (Rev. 8-98)
Prescribed by ANSI Std. Z39-18

Table of Contents

Preface

This technical report contains part of the work completed under the in-house project work unit 2301 S110, project title “Volume and Surface Plasmas”. Some of the earlier work was published in technical report # WRDC- TR-90-2027. The project engineer for this task is Dr. Biswa N. Ganguly. The research for this work was performed in the period 01 February, 1989 through 01September, 2004.

I. Introduction

This report describes work performed to obtain (1) scaling rules for the generation of low pressure nonequilibrium plasma for applications such as anisotropic plasma etching of wide band gap semiconductors, surface passivation of semiconductors devices for improved operating lifetime under high radiation flux environment; (2) energy efficient atom flux generator through multiquantum vibrational energy transfer in gas mixture plasma; (3) remediation of dust particles in rf plasma processing equipment; (4) self-assembled carbon nano-particle production in both reactive and non reactive plasmas through sputtering; (5) In-situ plasma and sheath electric field measurements in both volume and surface dominated plasmas by Rydberg State Stark Spectroscopy; (6) absolute atom density measurements by two-photon allowed laser induced in dc, rf, and microwave excited plasmas; (7) actinometric measurements of reactive atom density in rf etching plasmas; (8) strong double layer formation by weak shock propagation through nonequilibrium plasmas; (9) shock mitigation by plasma-shock interactions.

The main objectives of this project has been to develop methods for quantitative measurements of plasma properties which may permit to develop a scaling law for a specific application such as high flux atom source generator or surface damage free ion assisted etching of semiconductor materials with large cohesive energy. Similarly, for quantification of plasma- aerodynamic interactions, an electrically driven shock tube instrument was developed which permit simultaneous measurements of both gas dynamic and plasma properties modulated by the plasma-shock interactions. This approach has allowed us to quantify the relative efficiency of shock mitigation by plasmas through direct and indirect gas heating. The details of some of the recent research results are described in sections II, III, IV, V and VI. Also, other previous published research results that were published in the referred journal publications and as invited paper presentations are listed in the Appendix section. This in-house task has resulted into one issued patent one patent pending. Also, more than twenty journal publication and two book chapters have been written based on the research results obtained under this in- house task. Four Ph. D. theses were also sponsored.

II. Two color Mie scattering images of uncorrelated and correlated trapped dust in low frequency helium discharges.

We report measurements of self assembling of dust particles by their size distribution using simultaneous near real time two color Mie scattering in a 2 Torr pure helium, 15 to 20 KHz voltage excitation frequency, discharge operated with graphite electrodes. A 3 cm i.d. and 1 cm wide cylindrical graphite is used as outer electrode and a 1 cm diameter graphite is used as center electrode which are mounted in a 5 cm diameter glass tube (shown in figure 1). In this discharge configuration, the dust particles are transported by ion drag force to an equilibrium position just outside the interelectrode volume and they are trapped by the radial electric field. This condition leads to a minimum perturbation of the discharge electrical characteristics as the dust particle density grows. In pure helium discharge with graphite electrodes, the particle growth is primarily by ion accretion of sputtered carbon cluster ions. Ion accretion usually favors particle growth with a narrow size distribution[1]. This characteristic of the discharge permit us to follow the time evolution of trapped particles by their size distributions and also the transition of the particles from uncorrelated phase to a phase with long range correlation. A krypton ion laser output of 647.1nm and an argon ion laser output 514.5 nm are combined using a broadband half silvered mirror so that each beam is propagating parallel to each other but spatially displaced to permit chopping by the alternate blades using a mechanical chopper. A beam expander combination lens is used for both beams to illuminate a spatially overlapping wide discharge volume. A color video camera is used at 90 degree angle to detect the Mie scattered light from both laser beams at alternate video frame. A video frame grabber board is used for data transfer to a computer. Since the Mie scattering efficiency [2] scales as $(d/\lambda)^6$, where d is the particle diameter and λ is the scattered light wavelength, at a fixed scattering angle, the smaller particles will preferentially scatter 514.5 nm whereas the larger particles will scatter 647.1 nm. This arrangement permits imaging of self-assembled dust particle growth in both uncorrelated and correlated phases. Fig.1 and Fig. 2 (left) show the images of the trapped dust particles at the edge of the plasma after run time of several minutes. Note that larger particles (red scattered light) are assembled closer to the electrodes compared to the smaller particles. Also, the smaller particles are trapped and distributed over a larger volume compared to the heavier particles. The spatial variation of scattering intensities of both 647.1 nm and 514.5 nm show the dust densities are concentrated on or near the axis of symmetry with respect to the electrodes. Under this discharge operating condition, there is no measurable amount of dust particle trapped in the interelectrode volume due to the relatively strong radial electric field variation which permits transport of the negatively charged particles to the boundary walls.

After run time of tens of minutes, the Mie scattering intensities of both laser beam undergo a transformation from diffuse distributed light scattering to crisp objects with very well delineated boundaries, corresponding to the formation of highly correlated dust ensemble. Fig.1 and Fig. 2 (right), along with the blow up insets, show the Mie scattering

images of both scattered lights. These dust ensembles are located near the axis and correspond to the previous locations of highest dust densities, in the uncorrelated phase, which implies the presence of a very small radial electric field gradient. Also, the dust particles of same size are self- organized to form correlated ensembles.
Besides the characteristics of highly delineated boundaries, these dust ensembles exhibit very different dynamic behavior compared to the uncorrelated dust particles. The transport properties of these correlated dusts differ significantly from the uncorrelated phase during the discharge switch off. The uncorrelated dust particles undergo Coulomb explosion with the dispersal of the particles in all directions including against gravity. Whereas, the dust ensembles in the correlated phase retain their crisp boundaries for several video frames (> 0.1 sec) and their motion is determined primarily by the balance between the Stokes force and the gravitational force. This persistence suggests that in such dust ensembles the strongly correlated [3] ion- ion, and electron-ion motions lead to a several orders of magnitude reduction in the ion-ion and electron-ion recombination rates on dust particles compared to the ambipolar or to free diffusion conditions.

References:

1. P. Haaland, A. Garscadden, and B. Ganguly, Appl. Phys. Lett. 69, 904 (1996).
2. H.C. van de Hulst, "Light scattering by small particles"(Dover, New York, 1981), p 144.
3. V.N. Tsytovich, U.de Angeles, R. Bingham, and D. Resendes, Phys. Plasmas 4, 3882 (1997).

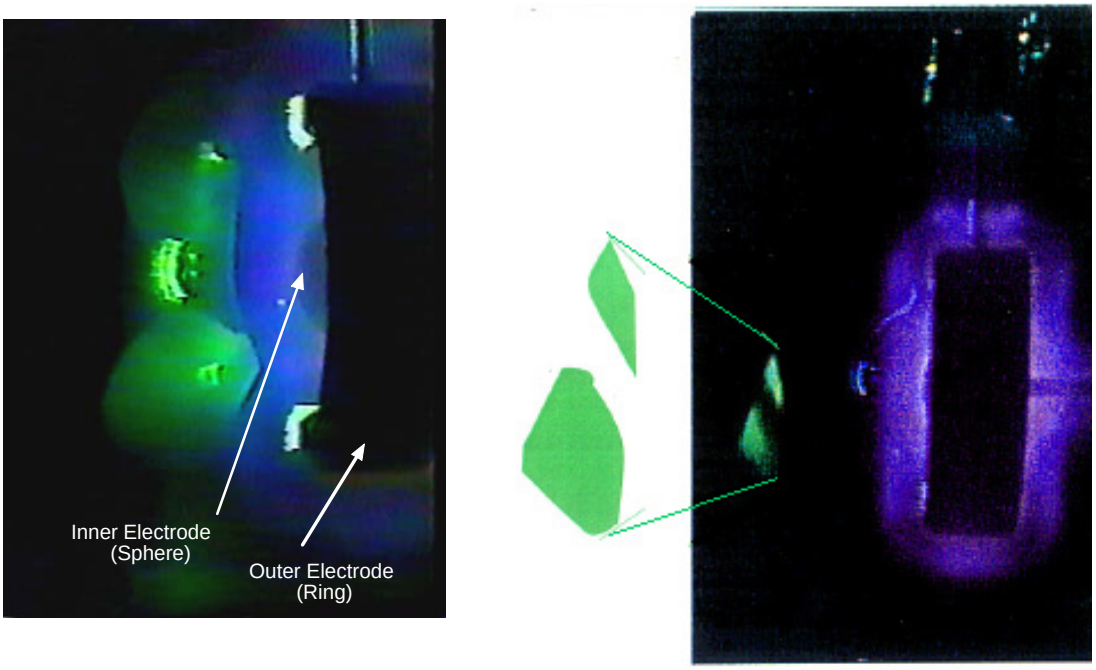

Fig. 1

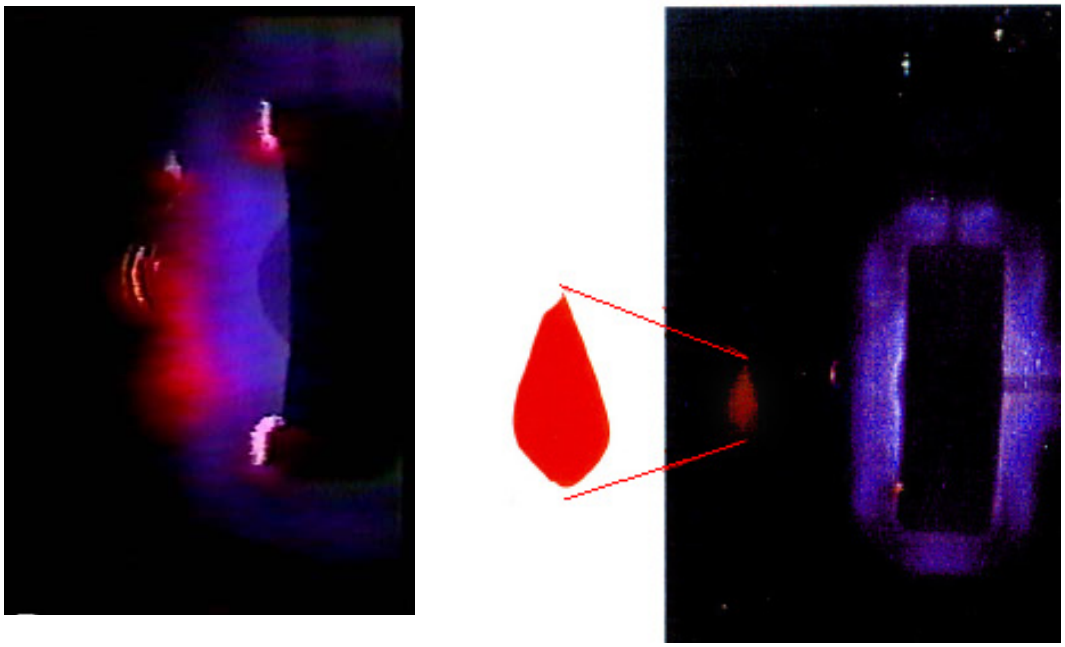

Fig 2.

Figure Captions:

Fig.1: Mie scattering image from uncorrelated (left) and correlated (right) dust using 514.5 nm laser beam.

Fig.2: Mie scattering image from uncorrelated (left) and correlated (right) dust using 647.1 nm laser beam.

III. The effect of displacement current on fast-pulsed dielectric barrier discharges.

1. Introduction

Dielectric barrier discharges (DBD) are in wide use for ozone generation, toxic gas remediation and surface treatment of materials. A conventional DBD uses high AC voltage at power line or higher frequency. The configurations may include a parallel or cylindrical electrode configuration with one or both electrodes covered with dielectric material. The breakdown of the gas under these conditions typically consists of a series of microdischarges at the positive and or negative peak of the applied voltage. The exact nature of these microdischarges is determined by the gas pressure, type of gas and the repetition frequency [1, 2] of the applied voltage. With certain gases such as He or N_2 and with the applied peak voltage only slightly above the gas breakdown voltage, the discharges may be limited to low currents, and this type of discharge may be in the form of an atmospheric glow discharge. The breakdown voltage at the operating frequency of the applied AC voltage determines the reduced electric field E/n (where E is the electric field, n the neutral gas density). Due to the buildup of surface charges on the dielectric barrier, the E/n decreases during the discharge[3] and may also decrease with consecutive micro-discharges. Plasma-chemical reaction rates (for processes such as excitation, dissociation) increase rapidly with increasing E/n and it is therefore desirable to operate the DBD at a high E/n for high plasma-chemical efficiency. It has been recognized [4, 5] many years ago that the high E/n could be achieved by operating the DBD with pulsed excitation. For example Lowther [4] used a 10 kHz, 0.8 μs 6kV pulsed DBD and claimed an ozone production efficiency of more than three times of that of a high voltage corona discharge with oxygen feed gas and almost six times that of dry air feed. Rosocha [5] used a parallel plate Blumlein pulser that also incorporated the discharge cell to investigate ozone production with pulses of up to 75 kV amplitude and risetimes as fast as 5 ns. Measurements and calculations of the effect of E/n in pulsed corona or pulsed DBD's show different results, in some cases because of different gas species. Some experimental results show an increase of chemical reactivity with E/n [4,6,7,8] and while others show no effect of increasing E/n [9,10,11].

The breakdown voltage using a pulsed voltage with short pulse width is normally higher than when using a slowly rising DC voltage, since the probability of an ionization event due to, for example, external radiation decreases with decreasing time interval. However introducing additional ionization, for example, by irradiation with a UV light source, can decrease the breakdown voltage of a pulsed discharge. If the pulse repetition rate is high enough so that there is remnant ionization from a previous discharge pulse, the pulsed breakdown voltage will also decrease. Therefore, remnant ionization in a repetitively pulsed DBD or external ionization will also influence the E/n of a DBD.

The time delay for the onset of breakdown after the application of the voltage pulse becomes shorter with increasing rate of voltage rise time, and with the decreasing delay time, the voltage at breakdown will also be higher for the faster rise times.

For applications using conventional circuit layouts, i.e. when the energy storage switch, conducting leads, and the discharge electrodes are not all part of impedance matched transmission line configuration, the circuit inductance and capacitance will have to be considered. Very early investigations of ozonizer discharges have already recognized this circuit effect [12]. The fact that the circuit components and in particular the electrode capacitance can have a considerable influence not only on the electrical characteristics but also on the plasma characteristics of the discharge is the subject of this note.

2. Experiment and electrical measurements

A photograph of the experimental layout used in our measurements is shown in fig. 3. A fast high voltage stacked CMOS switch is used to apply a shorting pulse to the top electrode of the two 1 x 10 cm copper electrodes straddling a 1 cm diameter discharge tube. The top electrode is charged to the high voltage via a charging resistor. The discharge tube is part of a vacuum system with electronic gas flow controllers and an automatic pressure controller. The pulse repetition rate could be varied from essentially zero to about 30 kHz. The discharge was operated at pressures from 30 to 200 Torr with a mixture of N_2/Ar (10:2) gas. At the highest operating pressure range, at 12 kV applied voltage across the 1 cm gap, breakdown required prior operation at lower pressure and a gradual pressure increase to provide remnant ionization. The capacitance of the electrodes was 27.5 pF, as determined from the electrical characteristics.

For a baseline estimate of the electrical parameters without a discharge, the current and voltage was measured at a pressure of 700 Torr and at the range of voltages used later when operating at lower pressure with a discharge. The measurements were then repeated at pressure of 50 and 100 Torr discharge, as shown in fig. 4. With a constant voltage of 12 kV and a constant pulse repetition frequency of 10 kHz, while the measured voltage essentially shows no change, the measured discharge current adds to the displacement current. As the pressure decreases, the gas breaks down earlier. This means that discharges at the lower pressures occur when the input voltage is at a higher value, so the discharge operates at a higher E/n. On the other hand the net current into the discharge is lower for the lower pressure. When the operating voltage is varied while keeping the pressure constant, a somewhat different behavior is observed. Figure 5 shows the discharge currents measured for different operating voltages and at 50 and 100 Torr pressures. For these figures the contribution of the displacement current for the respective operating voltage was subtracted so that only the net current into the discharge is shown. For both pressures, the current pulse amplitude increases for increasing operating voltage. The E/n of the discharge increases for increasing operating voltage not only because the operating voltage is higher but also because the onset of the discharge current occurs earlier and at a higher voltage. (However, the effect of increasing the operating voltage on the time delay decrease between the applied voltage and breakdown becomes smaller with increasing voltage and is practically absent at 50 Torr (fig.5)). The difference in breakdown time delay and pulse current amplitude for the two operating pressures is clearly shown in the inset of figure 5.

3. Optical measurements.

In order to investigate the effect of the measured electrical characteristics on the direct electron impact excitation in a gas discharge, the plasma emission intensity of three transitions in the 10:2 N_2/Ar gas mixture were measured. The three transitions were selected for their difference in excitation threshold which permits to estimate the variation of the tail of the EEDF, since the overlap of excitation cross sections and the EEDF are proportional to [13] $v_e^3 f_e(v_e)$, where v_e is the velocity of the electron and $f_e(v_e)$ is the electron energy distribution function. The net direct electron impact excitation rates[13] are a product of both the electron density and $v_e^3 f_e(v_e)$. The transitions were: N_2^+ B-X (band head at 391.4 nm, threshold 19 eV), Ar $2p_1$ to $2s_2$ 750.4 nm (threshold 13.5 eV) and N_2 C-B (threshold 11 eV). The operating pressure was varied from 30 to 200 Torr. A 1 m spectrometer with a Hamamatsu R758 photomultiplier was used. Figure 4 shows optical intensities (arbitrary scale) for the three transitions over the pressure range of 30 to 200 Torr. The transition with the highest excitation threshold, N_2^+ B-X, shows a steep drop with increasing pressure which is the expected behavior for a discharge with a few eV mean electron energy when the lowering of the E/n decreases the tail of the EEDF; therefore the overlap of excitation cross sections with the EEDF also decreases rapidly. The two electronic transitions with lower excitation threshold energy, Ar 750.4 nm line and N_2 C-B, both show an initial increase with increasing pressure. This is a clear indication of the increase of pulse current when the pressure increases, as demonstrated in fig. 4 and 5. The decrease in E/n is compensated, at least initially, by the increase in pulse current and power deposition. This effect is dependent on the excitation threshold of the particular transition. Since the N_2 C-B transition has a lower threshold than the Ar transition, it peaks at a higher pressure and it is less sensitive to a decreasing E/n. For the higher threshold N_2^+ B-X transition, the decreasing discharge E/n, even at the lowest pressure, impacts the direct electron impact excitation rate in spite of the increasing current because the overlap of the excitation cross section and the tail of the EEDF decrease faster than the electron density. These emission data clearly show the impact of increasing power deposition, even when the E/n decreases, with increasing pressure between 50 and 100 Torr. These optical emission measurements support the conclusions arrived from the time resolved electrical power deposition measurements and the estimated E/n values in a short pulsed dielectric barrier discharge.

4. Conclusions

With fast pulse excitation of a DBD the effect of the displacement current caused by the capacitance of the electrode structure cannot be neglected. For excitation processes with a low energy threshold, when the gas pressure is increased and the E/n is lowered, the increase in net current into the discharge can actually increase the direct electron impact excitation rate. The displacement current limits the increase of the discharge current when increasing the pulse voltage, since that also will increase the displacement current. For fast pulse DBD excitation, minimizing the electrode capacitance will lower the dielectric component of the charge current and the ohmic losses in a charging resistor, therefore increase the discharge excitation efficiency.

References:

1. B.Eliasson and U.Kogelschatz, IEEE Trans. Plasma Sci. 19, 309 (1991)
2. B.Eliasson and U.Kogelschatz, IEEE Trans. Plasma Sci. 19, 1063 (1991)
3. X.P.Xu and M.J.Kushner, J.Appl.Phys.83, 7522 (15 June 1998)
4. F.E.Lowther, U.S. patent 4016060 (1977)
5. L.A.Rosocha, PhD thesis, University of Wisconsin-Madison, (1979
6. J.J.Lowke and R.Morrow, IEEE Trans.Plasma Science 23, 661 (Aug.1995)
7. R.P.Mildren and R.J.Carmen, J.Phys.D:Appl.Phys.34, L1 (2001)
8. S.Liu and M.Neiger, J.Phys.D:Appl.Phys. 34, 1632 (2001)
9. B.Eliasson and U.Kogelschatz, J.Phys.B:At.Mol.Phys.19, 1241 (1986)
10. B.M.Penetrante, M.C.Hsiao, B.T.Merritt, G.E.Vogtlin, P.H.Wallman, M.Neiger, O.Wolf, T.Hammer and S.Broer, Appl.Phys.Lett. 68, 3719 (1996)
11. R.A. Korzekwa, L.A.Rosocha and Z.Falkenstein, IEEE 11th Intl. Pulsed Power Conference, Baltimore, Maryland,(1997)
12 .E.Warburg, Verh. Deutsch. Phys.Ges.5, 382 (1903) as quoted in R.W.Lunt, Adv.Chem. Ser.21, 287 (1959)
13. M.A.Lieberman and A.J.Lichtenberg, “Principles of plasma discharges and materials processing”, Wiley, 1994, p.258.

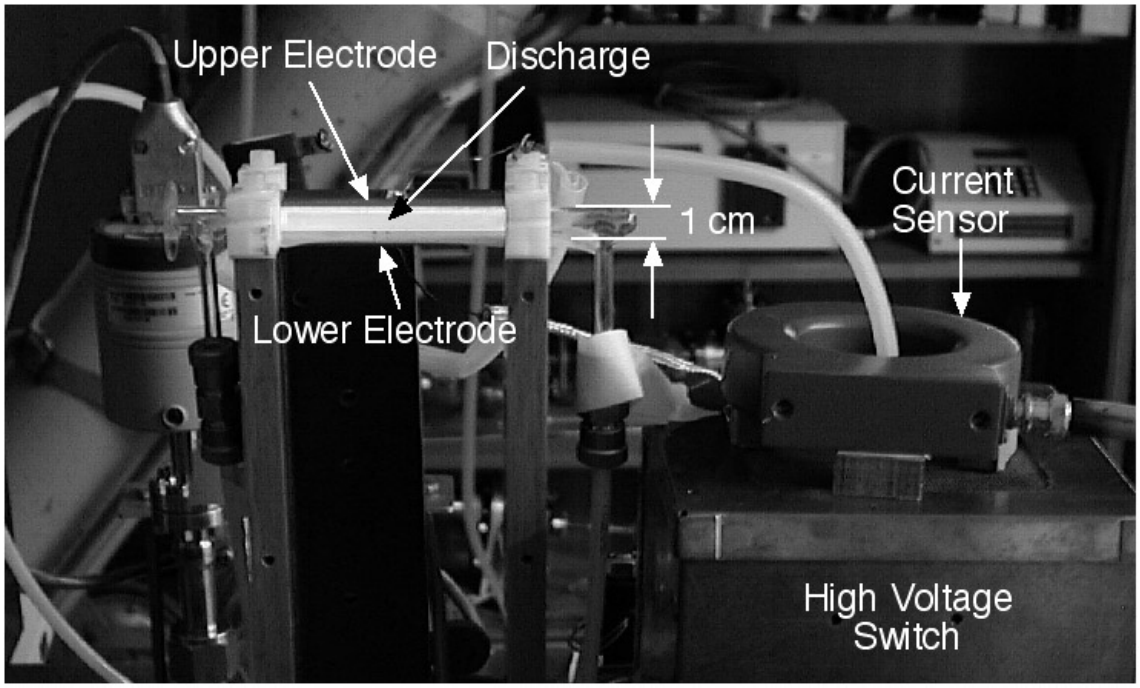

Figure 3. Photography of the DBD setup with pulser.

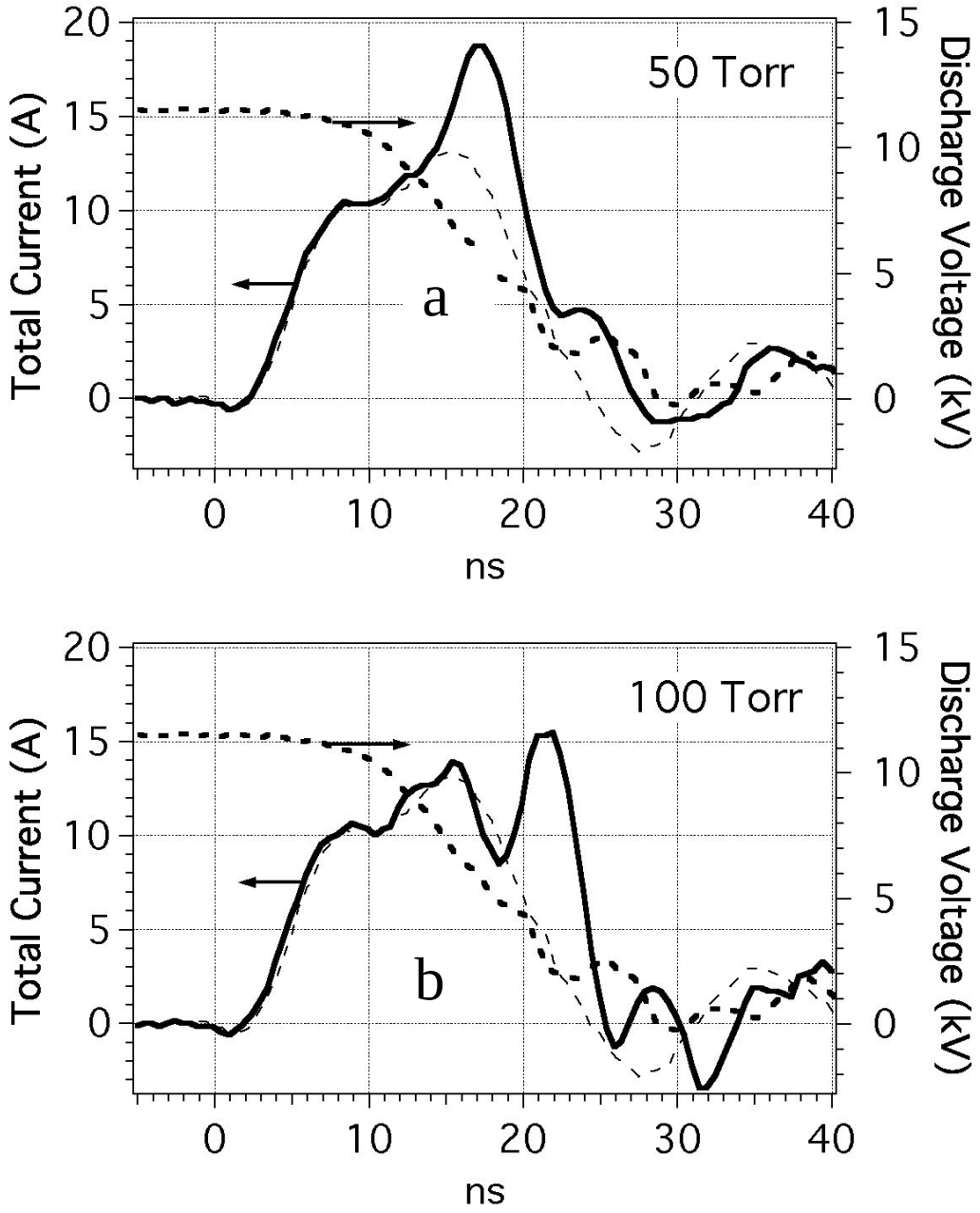

Figure 4. Discharge Voltage and discharge currents for two pressures for a N_2:Ar 10:2 gas mixture at 12 kV, 10 kHz. Zero time has been arbitrarily set to the beginning of the current pulse.(a) 50 Torr ; (b) 100 Torr. Thick line: Total current; Thick dashed line: Voltage. Thin dashed line: Displacement current only (700 Torr)

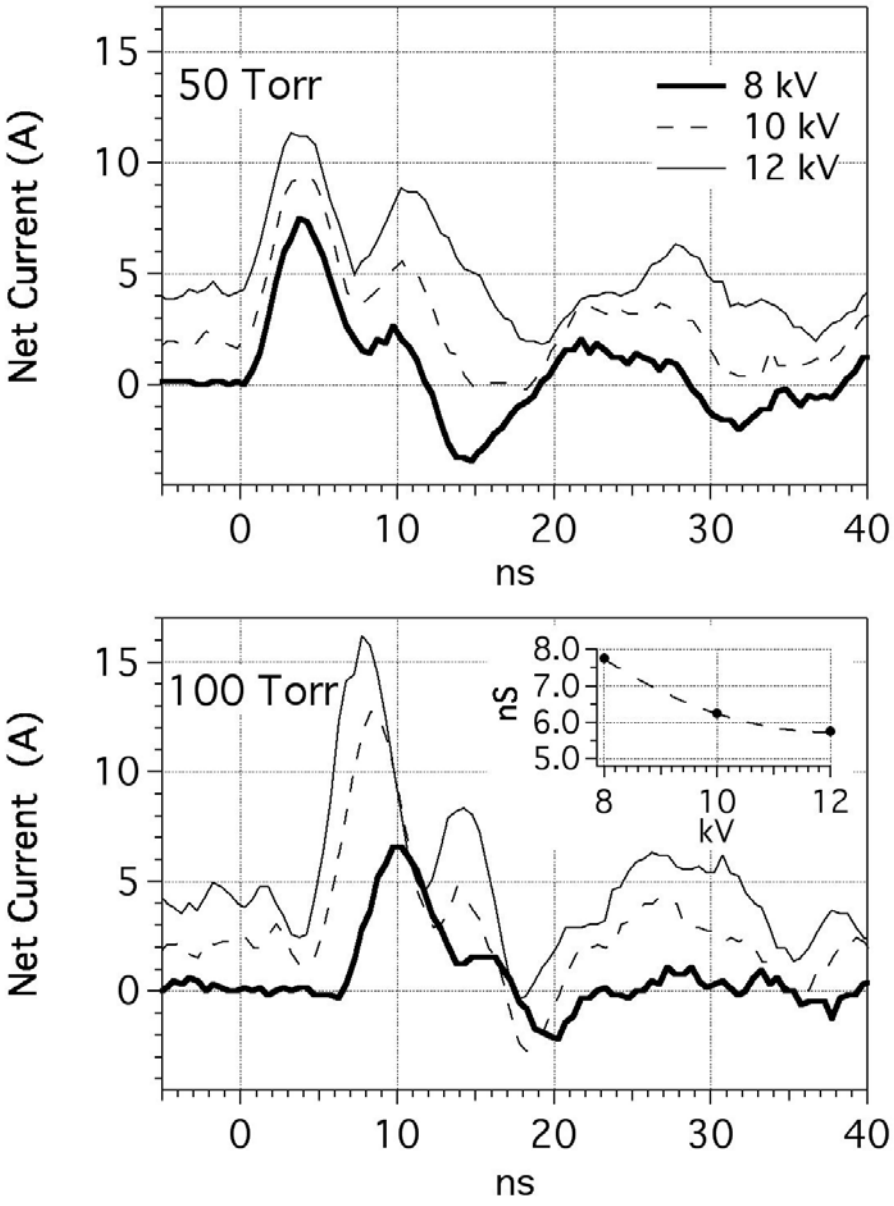

Figure 5. Net discharge currents (displacement currents subtracted from measured current) with N_2: Ar 10:2 gas mixture at 10 kHz and at different operating voltages. (a): 50 Torr, (b): 100 Tor. Thick solid line:8 kV, Thin dashed line:10 kV (shown vertically displaced). Thin solid line:12 kV (shown vertically displaced)The inset shows the delay of the current pulse as measured to the half amplitude versus the pulse voltage.

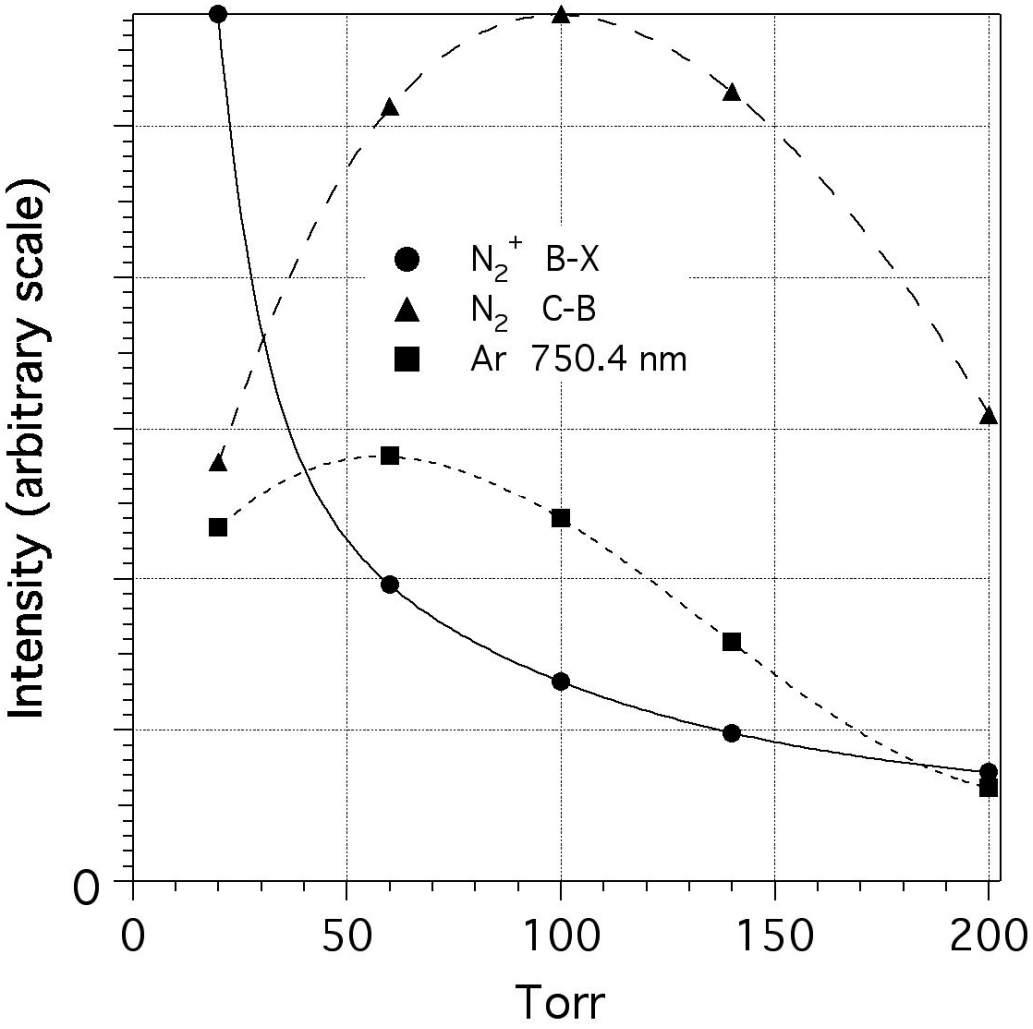

Figure 6. Optical emission intensities for N2 and Ar transitions for the same gas mixture at 12 kV, 10 kHz.

IV. Absolute H atom density measurement in a pure methane pulsed discharge.

In supersonic combustion (scramjet) systems the flow speed is very high so that mixing and reaction times are limited[1-3]. Some flow conditions also give rise to very low mixture temperatures[1]. For either condition, additional sources of ignition or combustion enhancement are needed. Plasma torch ignitors [1, 2] have been investigated widely, and microwave discharges[3] have been studied, both as means of providing reliable scramjet combustion. However, such approaches require multi-kilowatt electrical power inputs and are not easily volume scaleable. Highly nonequilibrium plasma production of energetic reactive hydrocarbon fragments could have application in situations where more conventional means of promoting and sustaining combustion are degraded [4, 5].

The attractiveness of high E/n, where E is the electric field and n is the gas density, pulsed discharges for dissociation, and electronic excitation and ionization is clear from both theoretical [6, 7] and experimental [8] work performed on corona and dielectric barrier discharges. Pulsed dc discharges in gaseous hydrocarbon mixtures can provide substantial amounts of atomic hydrogen, as well as electronically excited hydrocarbon fragment neutrals and ions. Such discharge products would be useful in promoting combustion in a wide variety of fuel to air mixtures.

The plasma volume and energy scaling of highly nonequilibrium plasma assisted ignition could improve overall efficiency of combustion. It is, therefore, important to quantify the radical production efficiency of a plasma device which could be used to replace a conventional spark ignition module. We have developed a short pulse excited discharge device [9] which can operate at high reduced electric field (E/n) with PD, P is the gas pressure and D is the gap distance, scaling up to 50 Torr.cm. Actinometric measurements performed in this high reduced electric field plasma device indicated that the CH_4 dissociation efficiency can be more than an order of magnitude greater than thermal dissociation process [9]. Although those measurements gave indications that a short pulse discharge can produce radicals with higher efficiency, compared to the thermal dissociation, those measurements were performed at low current density (2 Amp/cm^2) and low energy density (0.7mJ/cm^2). In this paper we report absolute H atom ground state density measurements in a short pulse methane discharge by two-photon allowed LIF (TALIF) technique at current densities exceeding 20 Amp/cm^2. The H atom TALIF intensity has been calibrated by comparing TALIF intensity from Kr atom ground state [10] to obtain absolute H atom density.

The goals of this study are: 1) construct a high E/n discharge system capable of producing discharges over a substantial range of input energy density, and 2) conduct spectroscopic measurements of the absolute H-atom production to estimate plasma dissociation efficiency of CH_4 in high E/n discharges. Pulsed gas discharges in CH_4 produce all possible methane fragments (CH_3, CH_2, CH, C and H) and their ions in varying ratios depending upon the discharge E/n. In the present study, we provide an accurate estimate of the direct electron impact dissociation efficiency of CH_4 in short

pulse excited, high E/n discharge, with nearly two orders of magnitude higher energy density compared to the previous measurement [9], using absolute H atom number density measurement by calibration of H atom TALIF signal with near isoenergetic Kr ground state atom TALIF measurement [10].

A solid-state, high-voltage, high-speed switch (15 kV, 30 A) provided a fast rise time voltage pulse and was controlled by timing control electronics. As shown in Figure 7, the voltage pulse was delivered (rise time <15 ns) via a microstrip transmission line to an end-fed coaxial section.

Four fused silica windows provided optical access. The discharge gap was viewed by a gated photomultiplier tube (PMT) fitted with an optical relay lens TL and preceded by F a long pass and a neutral density filter. The gated PMT allows photon detection after the plasma voltage pulse was turned off and the plasma emission had decayed. The laser was fired 185 ns after the voltage pulse was turned off. The pulse discharge and the TALIF data acquisition timing was controlled by a delay generator pulser and t=0 on all the data plots correspond to the start of the voltage pulse.

The 615 nm pulsed dye laser output tripled by a combination of KDP and BBO crystals and the TALIF emission was measured with a gated PMT. The optical path, including attenuation and collection solid angle, was kept fixed for all measurements. The laser beam was focused near the middle of the discharge volume and it was located 2 mm below the cathode surface for optimum TALIF signal. Absolute calibration used successive measurements of TALIF signals at two wavelengths; 205.08 nm probed the ground state of hydrogen atom produced by the pulsed discharge in methane and the 204.13 nm TALIF measured the calibration signal from the ground state of krypton atom.[10] These two probe wavelengths are close enough to ensure the input optics spectral throughput parameters remain constant. The 205.08 nm wavelength two-photon excites population of hydrogen atoms from the ground state, 1s, to 3d and 3s levels. The TALIF signal is detected by photon emission at 656.3 nm (H_α). The other probe wavelength excites a krypton transition from the ground state, $4p^6$, to $5p^/$ levels, using two photons at 204.13 nm and the emission from $5p^/$ to $5s^/$ was detected at 826.3 nm. For ease of calibration the two TALIF signals were set approximately equal amplitude by adjusting the pressure of Kr. A pyroelectric detector measurement was conducted with the series of TALIF measurements to assure that probe laser energy had not changed more than 5%, which limits the TALIF measurement error to 10% due to the laser intensity variation.

All measurements have been performed in pure CH_4 discharge at 20 Torr pressure with 5 mm gap between the 1 cm diameter electrodes. The applied voltage was varied from 4 kV up to 6 kV with 480 ns pulse duration. Gas flow and pressure was controlled by a mass flow controller loop using an exhaust valve controller and a mass flow readout, and a Baratron pressure transducer. Throughout this study the gas flow rate was fixed at 30 standard cubic centimeters per minute. The CH_4 gas was ultra high purity grade (99.999%).

The pulsed discharge voltage, and current deposited in the discharge are shown in Figures 8a, and 8b, respectively. The discharge voltage measurement of high speed pulses (<15 ns) show the gap voltage initially spikes, due to pre breakdown over volting, to a high value. At 6 kV applied voltage, the 20 Torr pure methane discharge runs at current density, j, up to 25 Amp/cm^2. The j/P^2 scaling of the cathode sheath voltage drop[11] for pure methane discharge is similar to that of H_2 discharge; the cathode fall voltage can be 700-750 V for these conditions. (Measurement of the discharge voltage using a variable gap discharge confirms the estimated sheath voltage drop). About 20 to 50 ns after breakdown, depending on drive voltage, a lower plateau gap voltage and the discharge impedance is established for the measured 480 ns voltage pulse duration. The discharge operating voltage is dependent on the initial applied voltage; it varies from 1100 V at 6 kV (sheath voltage drop 700 V) down to 900 V at 4 kV (sheath voltage drop 490 V). The corresponding volume average discharge E/n, assuming gas temperature is 400 K, can vary from 85 Td to 90 Td (1Td = 10^{-17} Volt cm^{-2}). The peak E/n, near breakdown, can exceed 300 Td.

Pressure dependent krypton TALIF calibration signal were measured and was found to be linear with pressure. Calibration transfer was made via a measurement at 0.318 Torr, where Kr signal amplitude was comparable to the H atom TALIF. A representative set of this series is shown in Figure 9 for three pressures 0.098, 0.191, and 0.318 Torr. Immediately following the Kr atom TALIF measurement, ground state H atom production in CH_4 discharge was measured.

The H atom TALIF intensity has been calibrated by comparing TALIF intensity from Kr atom ground state [10] to obtain absolute H atom density using the equation given below.

$$n_H = \kappa \frac{a_{23}(Kr)}{a_{23}(H)} \frac{\sigma^{(2)}(Kr)}{\sigma^{(2)}(H)} \frac{S_{PMT}(H)}{S_{PMT}(Kr)} \left(\frac{I_L(Kr)}{I_L(H)} \right)^2 n_{Kr} \qquad (1)$$

where n_H and n_{Kr} are the absolute number density of the H- and Kr-atoms respectively, κ is a transmission and sensitivity factor for the optical set-up and detector at the two wavelengths, a_{23} is the optical branching ratio ($a_{23} = A_{23} / \Sigma A_{2i}$, A_{23} is the spontaneous emission coefficient and ΣA_{2i} is the sum of spontaneous emission and collisional quenching coefficients), $\sigma^{(2)}$ is the two-photon cross section, S_{PMT} is the measured TALIF signal, and I_L is the intensity of the laser radiation. The ratio of the two-photon cross-sections, Kr atom optical branching ratio and collisional quenching rate of H atom 3d and 3s states by CH_4 are given in reference 10. Under our measurement conditions, the value of κ depends on the ratio of the PMT response sensitivity at 656.3 nm and 826.3 nm, which is obtained from the manufacturer's data sheet. Thus from a measurement of both the H-atom and Kr-atom TALIF signals, the absolute number density of H-atoms can be calibrated with a known number density of ground state Kr atom. Figure 10 shows H atom TALIF signals, calibrated in absolute H atom number density by comparing with Kr atom TALIF signal, obtained with three different applied drive voltages from 4 kV to 6 kV, with 480 ns pulse duration. The total input energy for these discharges were 6.5, 8.7, 11.4 mJ, respectively. For the corresponding discharge conditions, the measured H atom

density ranged from ~ 9.8×10^{15} per cm^3 at 4 kV to 2.2×10^{16} per cm^3 at 6 kV (TALIF pulse peak-to-area ratio is essentially constant so the peak values are used), i.e., nearly 4.5% of CH_4 was dissociated at 6 kV applied voltage, assuming 400 K gas temperature at 20 Torr, across the 5 mm gap discharge. Based on the energy deposited in the discharge volume near the cathode, an estimate of the direct electron impact dissociation efficiency of CH_4 +e → CH_3 + H +e can be obtained from the measured H atom yield in this pulsed discharge. The product of the direct electron impact dissociation rate coefficient and electron density in plasma is proportional to the fraction of discharge energy deposited to that process multiplied by the energy deposited in the gas, i.e.:

$$k_{ei}^{CH4} n_e^{CH4} \propto Y(E/n)\, P_{CH4} \qquad (2)$$

where $Y(E/n)$ is the fractional energy deposited into electron impact production of CH_3+H(n=1) as a function of E/n in methane discharges, k_{ei}^{CH4} is the electron impact dissociation rate, n_e^{CH4} is the electron density, and P_{CH4} is total discharge energy. For this discharge operating condition with 700 V sheath voltage drop along with about 80 V/cm plasma electric field in the 5 mm gap discharge, 70 to 75% of the energy is deposited in the discharge volume within 2 mm from the cathode surface. For the 6 kV applied voltage, discharge with 11.4 mJ total discharge energy, this would correspond to the discharge energy density ~ 70 mJ/cm^3. Assuming an average CH_4 dissociation energy cost of 10 eV, the total energy required to produce H atom density of 2.2×10^{16} per cm^3 would be 35 mJ/cm^3 (direct electron impact dissociation threshold[12] of CH_4 + e → CH_3 + H + e is 8.5 eV, and at the threshold energy the dissociation rate is very small. The higher dissociation rate, k_{ei}^{CH4}, with average electron energy cost of 10 eV would be more appropriate for this short pulse discharge). This would imply about 50% efficiency of the direct electron dissociation of CH_4 in this 6 kV short pulse discharge. Similarly for the 4 and 5 kV discharges, the corresponding energy densities are ~ 40 and 53 mJ/cm^3, respectively. The energy required to produce 9.8×10^{15} per cm^3 H atom density, at 4 kV, would be 15.7mJ/cm^3 and the CH_4 dissociation efficiency is ~ 40%. For the 5 kV discharge, the energy required to produce H atom density of 1.44×10^{16} per cm^3 would be 23 mJ/cm^3 and the dissociation efficiency is nearly the same as the 4 kV discharge. The measurable difference in the CH_4 dissociation efficiency at higher applied voltage may be caused by the increase in the discharge energy deposition in the sheath, where nonlocal electron impact excitation can dissociate CH_4 at higher efficiency than in the volume plasma. Note that volume plasma E/n is essentially constant for all the applied voltages. Although the importance of initial energy deposition near the breakdown under higher E/n can not be directly quantified from these measurements, these measurements clearly show the advantage of operation at higher applied voltage even for a relatively long pulse duration discharge compared to the initial high peak power pulse duration. In summary, we have used absolute H atom density measurements by TALIF to demonstrate high efficiency operation of short pulse excited discharge for CH_4 dissociation, H atom and CH_3 radical production which can be used for ignition and combustion enhancement for high speed propulsion.

References:

1. T.C. Wagner, W.F. O'Brien, G.B. Northam and J.M. Eggers, J. Propulsion 5, 548 (1989)
2. T. Mitani, Combust. Flame 101, 347 (1995).
3. K. Khodataev and A. Ershov, in 2nd Weakly Ionized Gases Workshop, Proceedings Supplement, Norfolk, VA, p. 341-350, (1998).
4. Y. Y. Buriko, V. A. Vinogradov, V. A. Goltsev, and P. J. Waltrup, J. Propulsion and Power 18, 1049 (2002).
5. S. A. Bozhenkov, S. M. Starikovskia, A. Yu. Starikovskii, Combustion and Flame 133, 133 (2003).
6. R. Dorai, K. Hassouni, and M. J. Kushner, J. Appl. Phys 88, 6060 (2000).
7. V. Puchkarev and M. Gundersen, Appl. Phys. Lett. 71, 3364 (1997).
8. R. S. Sigmond and M. Goldman in Electrical breakdown and discharges in gases eds.E.E. Kundhart and L. H. Luessen, Plenum, New York, 1981, pp 1-64.
9. S. D. Marcum, J. W. Parish, and B. N. Ganguly, J. Propulsion and Power (to be published).
10. K. Niemi, V.S. von der Gathen, and H. F. Dobele, J. Phys. D: Appl. Phys. 34 2330 (2001).
11. A. von Engel, Ionized Gases, American Institute of Physics, New York, 1995, pp 222-236.
12. R. K. Janev, and D. Reiter, Phys. Plasmas 9, 4071 (2002).

FIGURES

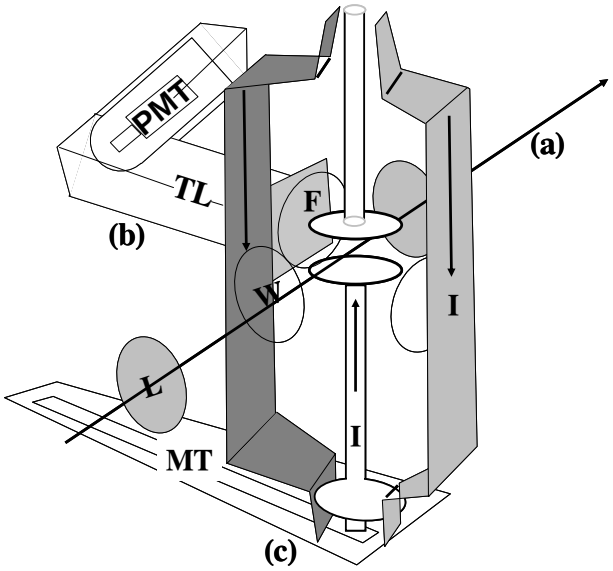

Figure 7. An experimental schematic; a) laser beam path through a focusing lens L and quartz windows W, b) a housed PMT with a view of the gap orthogonal to the beam through transfer lenses TL and long-pass/neutral density filters F and c) a microstrip transmission line MT feeding the gap on center of a symmetrical pair of cylindrical section copper conductors, the conventional current I is shown with arrows.

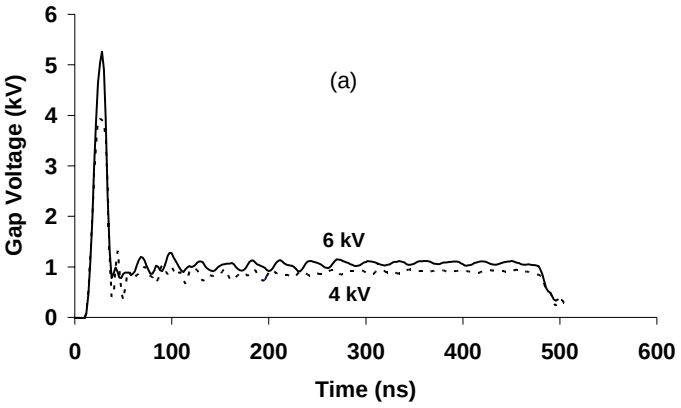

Figure 8a. Discharge gap voltage for 480 ns pulse width 4 and 6 kV applied voltages across a 5 mm gap, 1 cm diameter electrodes, at 20 Torr CH_4.

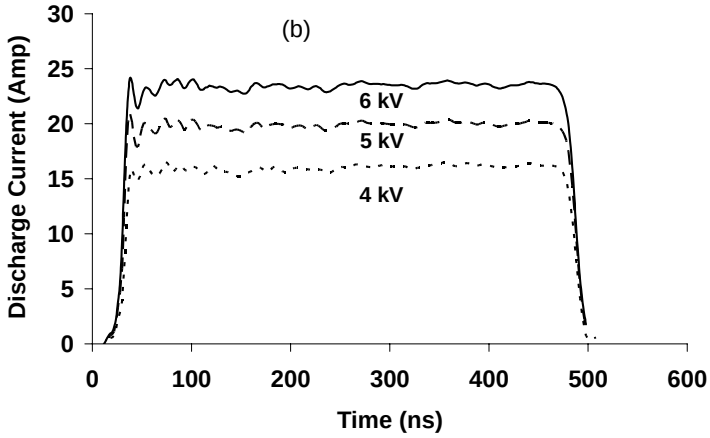

Figure 8b. Discharge current pulses for 480 ns pulse width 4, 5, and 6 kV applied voltages, across a 5 mm gap, 1 cm diameter electrodes, at 20 Torr CH_4.

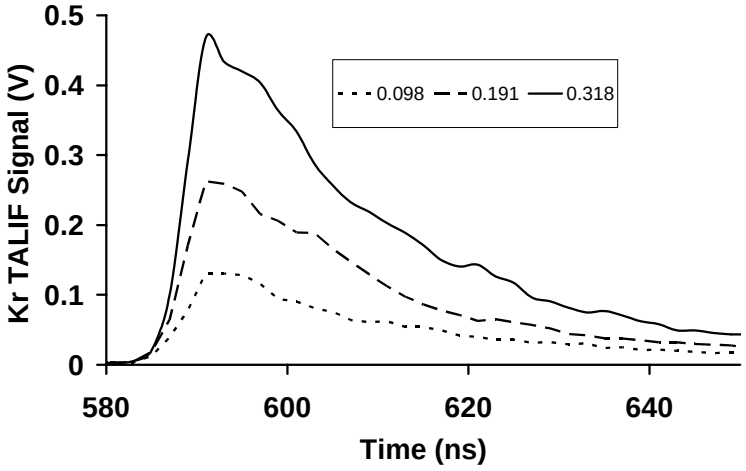

Figure 10. Krypton atom calibration TALIF measurements for Kr gas pressures 0.098, 0.3191, and 0.318 Torr.

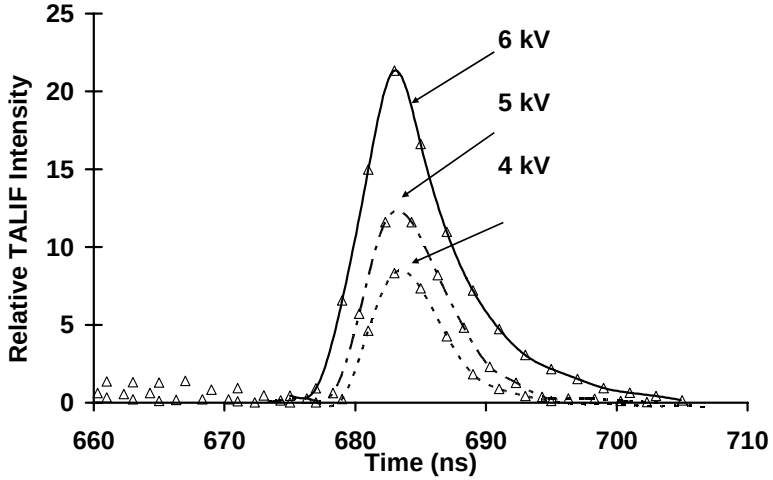

Figure 11. TALIF measurement of absolute H atom density in 20 Torr, 480 ns pulse width, CH_4 discharge with 4, 5, and 6 kV applied voltages. Absolute H atom densities are obtained from the Kr atom TALIF calibration, yielding H atom density of 9.8×10^{15} per cm^3 at 4 kV, 1.44×10^{16} per cm^3 at 5 kV, and 2.2×10^{16} per cm^3 at 6 kV.

V. Evidence of enhanced electronic excitation at the shock front of low Mach number shocks in non-equilibrium plasmas

The propagation and dispersion of weak shock waves in non-equilibrium plasmas have recently received considerable attention [1-6]. Optical and pressure probe measurements show spreading of the shock front and an increase in shock velocity in the plasma. Some investigators relate these effects to axial or radial thermal gradients[4,5] in the plasma, others invoke effects caused by a shock wave induced electrostatic interactions [1,3] in the plasma. Depending on the boundary conditions of the experiments, these interpretations may be applicable. We have recently investigated [6] the interaction of the shock wave with the N_2 plasma in a DC glow discharge and have shown that the propagating shock wave causes large local changes in the electric field in the immediate vicinity of the shock front as well as global changes in discharge voltage and current. The magnitudes of these effects were shown to be dependent on discharge polarity. Spatially and temporally resolved measurements of the optical emission from the $C^3\Pi_u$ - $B^3\Pi_g$ transition in nitrogen showed sharp decreases when the shock wave passed through the observation point. Fig. 12 shows a series of ICCD camera images taken with a 1.2 μs exposure time and a blue filter, which eliminates the emission of the nitrogen recombination afterglow. The ICCD pictures were made on a 5 cm diameter, 5 Torr, 60 mA discharge.

As the shock wave sweeps through the positive column, the discharge becomes dark behind the shock. This result indicates a significant decrease in the reduced electric field E/n, where E is the electric field and n is the neutral density, behind the shock even though there is continuity of current. Note also that the emission intensities near both the cathode and the anode show no discernible change in intensity, confirming that under these operating parameters the discharge current changes little. These observations are correlated with an observed sharp decrease of the reduced electric field at the shock arrival time as measured by electrical probes [6]. The decrease in optical emission to practically zero intensity behind the shock front indicates a reduction of electron impact excitation and therefore also of ionization. As already observed from the ICCD images of the cathode and anode glow, the discharge current decreased only moderately during the time when the shock passed through the length of the positive column discharge tube for anode to cathode propagation. It even showed a small temporary increase for shock propagation in the direction from cathode to anode. The decrease of electronic excitation and ionization could be explained by the large increase of neutral density behind the shock front and therefore a decrease of E/n. However, the decrease of E/n with the increase in neutral density will also reduce the electron drift velocity. Therefore, discharge current continuity requires an increase of electron density, compensating drift velocity decrease, by a factor of 2 for the Mach 1.7 shock waves. The observed sharp drop in the local electric field propagating with the shock front indicated a local region of enhanced conductivity [6]. This abrupt change in electric field (requires net space charge to satisfy Poisson's equation) suggested the formation of a triple- or quadruple space charge layer connected with the shock front. The high electric fields in this very localized space charge region, ahead of the shock front, can then lead to local (dimension determined by the plasma Debye length) excitation and ionization that can provide the excess electron density. The calculated electron density decay in an equivalent unperturbed positive

column discharge was estimated to be at most 20% during a time equal to the shock traversal time.

The optical and electrical measurements gave a self-consistent picture of the plasma-shock wave interactions and the new measurements reported here provide evidence for the presence of strong excitation (and ionization) enhancement in a very narrow region propagating with the shock wave.

Under the conditions of the discharge (5 Torr, 50-100mA), the upstream neutral gas mean free path (temperature corrected) is 0.005cm and the estimated Debye length for the largest current is 0.01cm [6]. Assuming that the increase in optical emission will occur over the Debye length connected with the plasma conditions of the passing shock front, it will have a width of less than 0.3 mm. The spatial resolution requires that the full width of the discharge be within the depth of field of the photomultiplier optics. Taking a discharge diameter of 4 cm, on the outer limits of the diameter of the discharge, the optics used (f number 30, 90 mm focal length) will allow a resolution of only 1.7 mm (or blur disc diameter)[7]. A resolution of 0.1 mm is possible over a depth of field of 2.4 mm only. The combined effects of short radiation enhancement time and insufficient spatial resolution will broaden the pulse width of a shock induced enhanced optical radiation pulse and reduce its amplitude, making its detection difficult. These limitations may have been responsible for our inability to detect the expected electron impact excitation enhancement in C to B emission.

In order to improve our plasma emission detection sensitivity, we have measured the 2-0 vibrational transition of the $B^3\Pi_g - A^3\Sigma_u^+$ first positive band, which has a radiative lifetime of 8.46 μs [8]. This longer lifetime along with the lower excitation energy level compared to the $C^3\Pi_u$ state was expected to give a better chance to observe the enhanced emission peak at the shock front. The B state can also be populated by cascading from three other states. The experimental setup, except for the spectral filter and a 3 cm diameter discharge tube with electrodes conformal with the glass wall, was identical to the one used previously [6]. This discharge geometry permits shock wave propagation measurements with the discharge polarity reversed with minimal modification of the test setup. The tube diameter was 3 cm diameter vs. 5 cm in the previously reported measurements [6], and at 3 Torr, the Mach number is about the same than in the previous measurements (Mach 1.76) using 100 Joules spark gap energy input. The narrower tube diameter and lower pressure also results in increased electron losses to the wall in this diffusion-dominated discharge so the electron mean energy is slightly higher than in the discharge of our previous report[6]. The optical observation point was 118 mm from the electrode closer to the spark gap and the distance between the electrodes was 180 mm. Fig. 13a shows the discharge voltage, current and 775.4 nm emission for a shock wave propagation from cathode to anode, fig. 13b from anode to cathode, in both cases for a DC current of 20 mA at 3 Torr. The laser photo deflection markings of the shock front arrivals[6] in the 775.4 nm emission diagrams are for the physical location of the photomultiplier. The time period during which the shock wave traverses the discharge is indicated by the vertical dashed lines. As observed previously, the discharge voltage decreases and the current increases by 10% for about 100 μs for cathode to anode shock propagation direction, for the opposite propagation direction the voltage increases and the current decreases immediately. Again as previously observed, locally at the photomultiplier observation point the light intensity increases when the

shock wave enters the discharge for cathode to anode propagation and decreases for the opposite propagation direction. The electrical as well as the optical effects, before arrival of the shock at the observation point, are caused by the global electrical circuit response to the propagating shock wave, as described previously [6]. The global voltage and current perturbations in this smaller diameter, lower pressure discharge are larger than for the previous measurements [6]. A sharp and pronounced peak of 775.4 nm emission is observed when the shock wave passes through the observation region for both propagation directions. The emission peaks have a rise time of 2 μs and a decay time of about 40 μs. This long decay is in contrast to the 337.1 nm emission observed previously, which decays within less than 2 μs to practically zero intensity in conjunction with the fast increase in neutral density behind the shock. The long decay time is probably caused by the heavy particle collision induced excitation[9] of the B state due to the reaction $N_2(A^3\Sigma_u^+)+N_2(X^1\Sigma_g^+,v\geq5) \rightarrow N_2(B^3\Pi_g)+N_2(X^1\Sigma_g^+)$. (Both the $A^3\Sigma_u^+$ state and the vibrationally excited ground state have long life times).

The rapid rise in intensities of the 775.4 nm emission is an indicator of a large increase in electronic excitation rate connected with the shock wave induced very local increase in E/n value (or electronic energy distribution function). Due to the limitations of the optical system mentioned above, the temporal width of the rising portion of the measured 775.4 nm radiation pulses, which corresponds to the apparent duration of the shock wave generated local increase in E/n pulses, is much longer than the actual width of these radiation pulses and also the duration of the increased electronic excitation. For the same reason, the amplitudes of the measured pulses are much smaller than the actual radiation amplitudes. For this positive column discharge [6], which runs at E/n ≈ 45 Td (1 Td= 1×10^{-17} V cm^{-1}), the observed $B^3\Pi_g - A^3\Sigma_u^+$ intensity jumps by at least 20% compared to the steady state in 2 μs. This requires a rate of change of the electron impact excitation by a factor of 10^5 indicating that the E/n increases [10] from 45 Td to > 240Td. The decay of the 775.4 nm radiation is strictly due to the population transfer from long-lived states after the short period of direct electron impact excitation enhancement; no such long decay was observed with the 337.1 nm radiation since the C state is populated primarily by direct electron impact.

In fig. 14 the emission signals from the C to B and B to A states are compared. The photomultiplier output traces are aligned such that the signal amplitudes before arrival of the shock wave are about equal on the plot. The rise of the 775.4 nm signal corresponds to the arrival of the shock wave, and the decay of the 337.1 nm signal to the departure of the shock wave from the observation point. Due to the limitations in spatial resolution discussed above, the half width between the two signals is about 2 μs, which would correspond to a width of the shock wave of ≈ 1 mm at a velocity of Mach 1.76. As discussed above, the actual width is probably more than an order of magnitude smaller. The decay of the discharge current follows an exponential function. While this dependence usually indicates ambipolar diffusion decay to the wall, the decay time constant is smaller than expected from a plasma with an estimated electron temperature of about 0.3 eV at the elevated pressure after the shock. We may assume that some of the charge carriers leave through the ends of the discharge since in this experiment, unlike in a conventional pulsed afterglow, there is still an applied electric field. However the E/n is much reduced and too low for efficient ionization. Therefore, even with reduced drift velocity, the current to the discharge electrodes still will cause additional plasma loss.

The observed B to A emission enhancements show that the postulated [6], triple or quadruple space-charge layer connected with a shock wave propagating in non-equilibrium plasmas can induce strong local electronic excitation. We are presently investigating the consequence of the increase in local E/n on ionization enhancement, and also the local Joule heating that could be generated, at or near the shock front, by such an ionization enhancement produced by the shock induced space-charge layer formation in a nonequilibrium plasma.

References:

1. G.I.Mishin, A.P.Bedin, N.I.Yushchenkova, G.E.Skvortsov, A.P.Ryazin, Sov.Phys. Tech.Phys. 26, 1363 (1981).
2. I.V.Basargin, G.I.Mishin, Sov.Tech. Phys.Lett. 11, 85 (1985)
3. A.Yu. Gridin, A.I..Klimov and N.E. Molevich, Sov. Phys. Tech. Phys. 38, 238 (1993).
4. P.A.Voinovich, A.P.Ershov, S.E.Ponomareva, V.M.Shibkov, High Temp. 29, 468 (1990)
5. Y.Z. Ionikh, N. V. Chernysheva, A. V. Meshchanov, A. P. Yalin and R.B. Miles, Phys. Lett. A 259, 387 (1999).
6. P. Bletzinger, B.N. Ganguly and A. Garscadden, Phys. Plasmas 7, 4341 (2000).
7. G.Franke ," Physical Optics in Photography" (Focal Press, London, 1966) p31-32
8. L.G.Piper, J. Chem. Phys. 91, 864 (1989).
9. L.G.Piper, K.W.Holtzclaw, and B.D. Green, J. Chem. Phys. 90, 5337 (1989).
10. K.Behringer and U.Fantz, J.Phys. D 27, 2128 (1994).
11. J.Loureiro and C.M.Ferreira, J.Phys. D 22, 67 (1989).

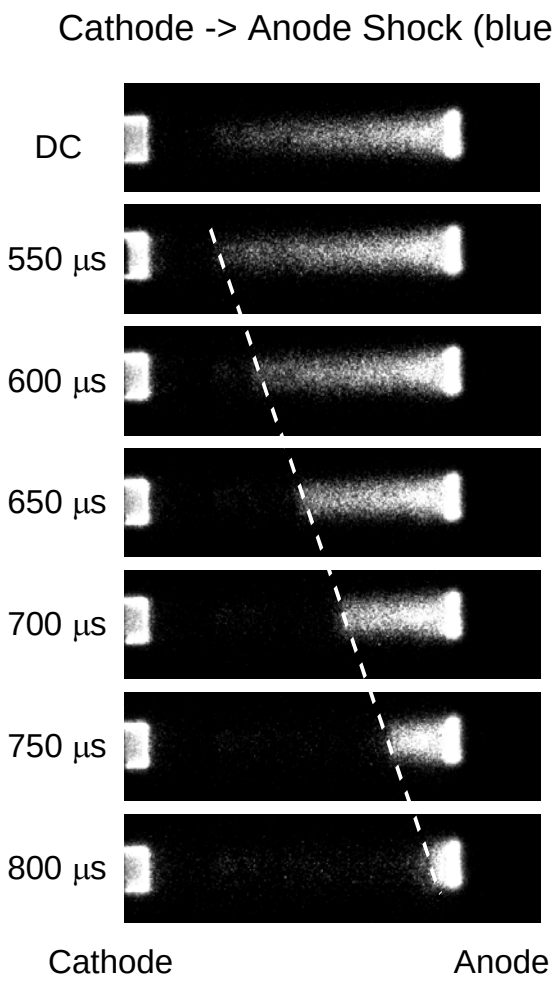

Figure 12: ICCD camera pictures of the positive column light emission response of a N_2 discharge (5 Torr, 60 mA discharge current, 1.2μs exposure time, blue filter, tube diameter 5 cm) to a shock wave entering from the lhs of the photographs. The progression of the shock wave from cathode to anode is approximately indicated by the dashed line.

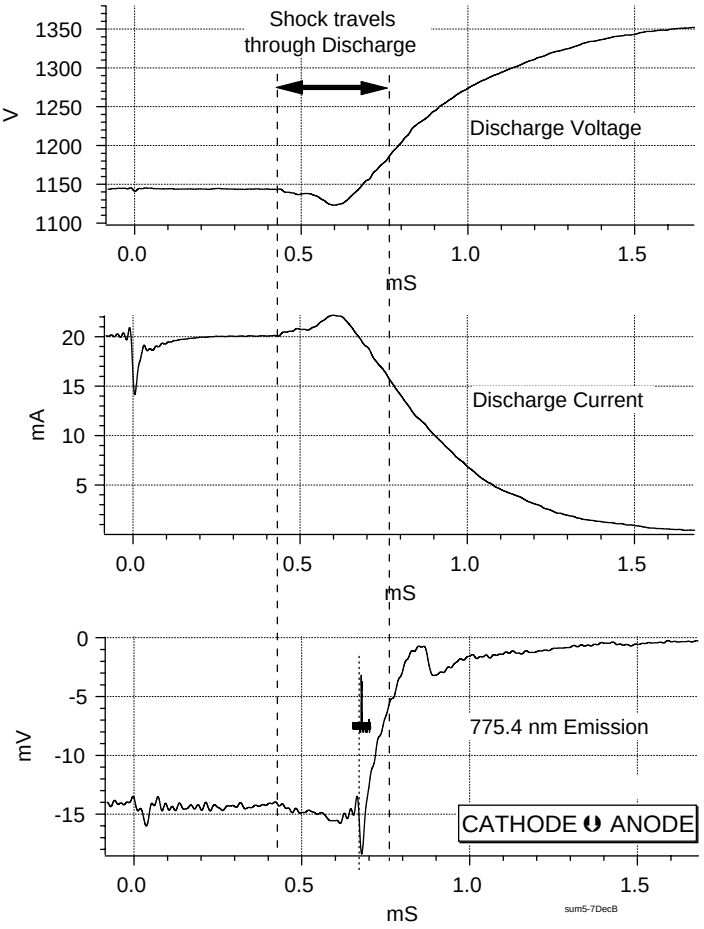

Figure 13a: Discharge voltage, current and 775.4 nm emission in a 3 Torr, 20 mA discharge in N_2 for a shock propagating from cathode to anode. A laser photodeflection signal for the location of the photomultiplier is shown in the 775.4 nm emission diagram. The time during which the shock traverses the discharge is indicated. (Photomultiplier intensity increases downwards).

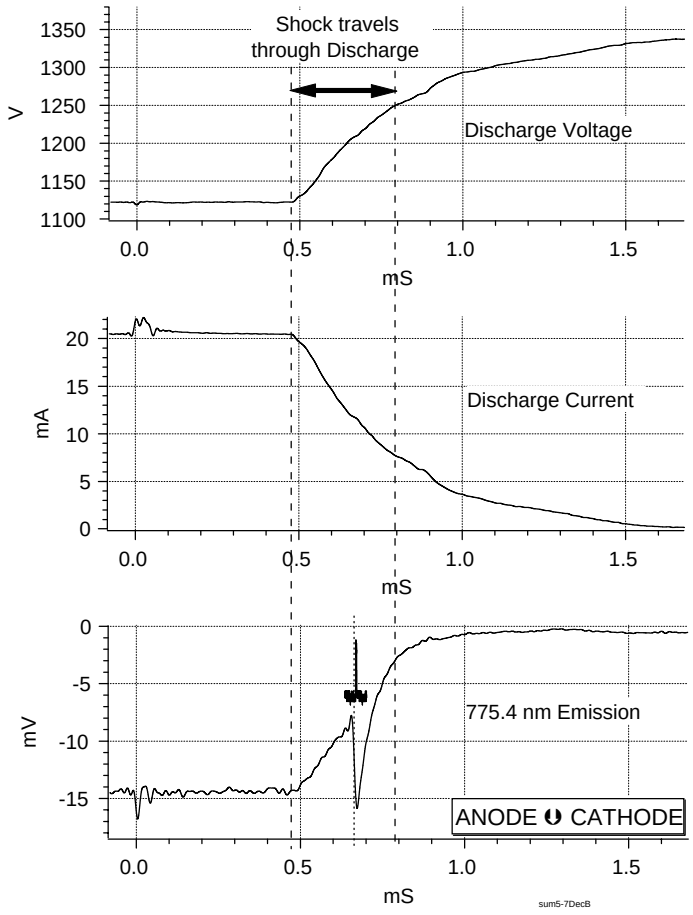

Figure 13b: Same as figure 2a but for anode to cathode shock propagation.

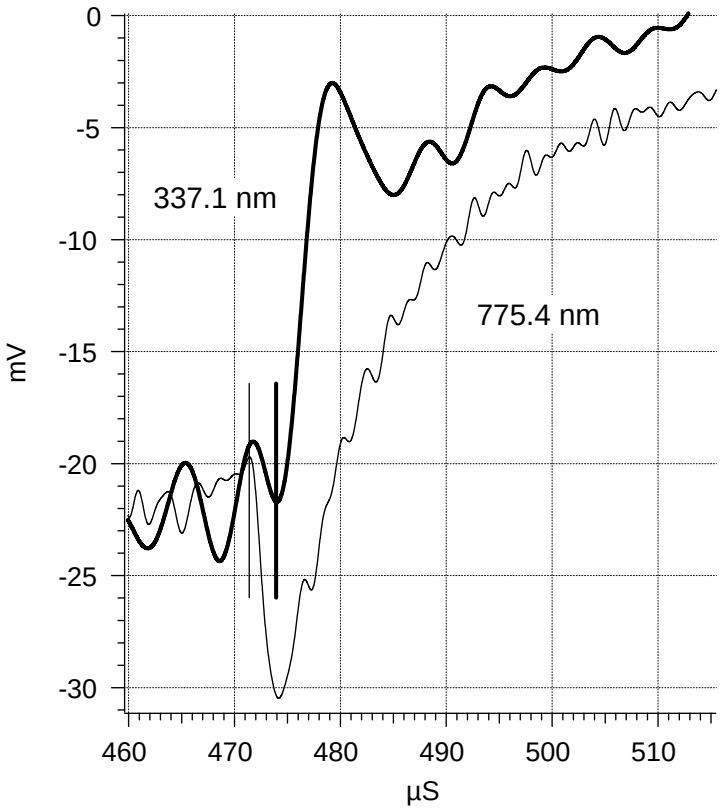

Figure 14: Comparison of 337.1 nm and 775.4 nm emission signals for the same conditions as in figure 2a. The scales for each signal are adjusted such that the signal amplitudes before arrival of the shock are equal. The 775.4 emission increase correlates with the arrival of the shock wave at the observation point, the 337.1 emission decrease with the departure. The vertical markers indicate the time difference between the enhanced excitation (B-A), increased E/n signal and the signal decrease (C-B) caused by the density jump.

VI. Methane Dissociation in Pulsed DC Discharges at High E/N

Nomenclature

E - electric field magnitude
N - gas number density
E/N - reduced electric field measured in Townsends (Td)
(note: 1 Td = 10^{-17} V cm^2 = 0.323 V/Torr cm at 300 K)
XY(state label $^{\text{multiplicity}}_{\text{parity}}$) - generic molecular electronic state designation
v - change in vibrational quantum number
p - pressure
d - discharge gap
n - principal quantum number
gas - hydrogen or methane
X(E/N) - fraction of discharge power deposited into dissociation as a function of E/N
P_{gas} - discharge power deposited into a given gas
D_e - energy required for dissociation
V - discharge volume
t - time
$I_{H\alpha}^{gas}$ - intensity of H emission from a given discharge gas
C - constant containing all detection system optical and geometrical parameters
h . - photon energy for H(n=3 to 2) or H emission
A_{32}, A_{3j} - Einstein coefficient for spontaneous emission for the indicated transition
k_e^{gas} - electron impact dissociative excitation rate coefficient
n_e^{gas} - electron density in a given discharge gas
k_Q^{gas} - quenching coefficient for H(n=3) atoms in a given gas
$[H_2]$ - concentration of molecular hydrogen
$[CH_4]$ - concentration of methane
E_{th}^{gas} (*DE*) - threshold for dissociative excitation to H(n=3) for a given discharge gas
E_{th}^{gas} (*D*) - threshold for dissociation of a given discharge gas
k_{ei}^{gas} - rate coefficient for electron impact excitation to H(n=3) for a given discharge gas
$[H]_{gas}$ - concentration of H atoms in a given discharge gas
Y(E/N), Y'(E/N) - fraction of discharge power deposited into electron impact excitation as a function of E/N

Introduction

Atomic hydrogen, hydrocarbon fragments and their radicals are important species for initiating ignition and sustaining stable flame propagation. Molecular gas discharges generally give rise to a complex set of interactions between atoms, internally excited molecules and radicals. Globally, discharge power is deposited via inelastic electron

collisions into molecular species as rotational, vibrational or electronic excitation, and via dissociation or ionization. Clearly the various channels compete for discharge energy, with the fractional power transferred to each being a strong function of E/N (where E is the electric field and N is the gas density). At low E/N rotational and vibrational excitation typically dominates. As the discharge E/N is increased, dissociation, electronic excitation and ionization collectively share the bulk of the input discharge power[1, 2]. Highly nonequilibrium plasma production of energetic reactive hydrocarbon fragments could have application in situations where more conventional means of promoting and sustaining combustion are degraded.

One such situation is found in supersonic combustion ramjet (Scramjet) propulsion systems where the flow speed is so high that mixing and reaction times are limited[3-6]. Some flow conditions also give rise to very low mixture temperatures[3]. For either condition, additional sources of ignition or combustion enhancement are needed. Plasma torch ignitors[3] have been investigated widely, and microwave discharges[5] have been studied, both as means of providing reliable Scramjet combustion. However, such approaches require multi-kilowatt electrical power inputs and are not easily volume scaleable.

The efficacy of the plasma torch approach is attributed to the introduction of atomic hydrogen[3] into the flow. A plasma torch, typically using a flowing Ar-H_2 mixture, operates at low E/N and acts to *thermally* dissociate hydrogen in a low E/N arc discharge. Hence the energy requirement is high. Pulsed dc glow discharges with high E/N in pure H_2 and H_2-N_2 mixtures[1,2] have demonstrated efficient dissociation of hydrogen with substantially lower power requirements. The attractiveness of high E/N pulsed discharges for fostering dissociation, electronic excitation and ionization is clear. Pulsed dc discharges in gaseous hydrocarbon mixtures similarly provide substantial atomic hydrogen, as well as electronically excited hydrocarbon fragment neutrals and ions. Such discharge products would be useful in promoting combustion in a wide variety of fuel to air mixtures. Additionally, control of discharge parameters offers the possibility of varying the yields of the dominant reaction products in response to changing conditions in an application.

Discharges in methane and methane-bearing mixtures have been the focus of a number of recent studies with a variety of potential applications. For example, pulsed discharges in methane have been shown to provide efficient conversion to acetylene and hydrogen.[7, 8] Similar discharges have been employed for plasma carburizing of surfaces[9] and for the production carbon-based nanoparticles[10, 11].

The primary goals of this study were: 1) construct a discharge system capable of producing uniform methane discharges over a substantial range of high E/N values, and 2) conduct imaging and spectroscopic measurements of the resulting plasma emissions sufficient to document plasma uniformity, and provide an estimate of H-atom production. Pulsed gas discharges in CH_4 produce all possible methane fragments (CH_3, CH_2, CH, C and H) and their ions in varying ratios depending upon the discharge E/N. Additionally, some carbon clustering occurs[9-11]. Of these, excited neutrals of atomic hydrogen, CH and

C_2 were chosen for spectroscopic observation due to their easily detected visible emissions (H at 656 nm, the CH (A^2 - X^2) band at 431 nm, and the C_2(A^3 $_g$ – X^3 $_u$, v = 0) Swan bands near 516 nm[12,13]). Comparison of H. emissions in the CH_4 discharges with that of the much better characterized H_2 discharges[1, 2, 14-16] provides the desired H-atom production estimate. The correlation of bright C_2 band emission with discharge inhomogeneity is also documented and discussed. The issue of discharge homogeneity may be important primarily from the viewpoint of further studies involving laser spectroscopic measurements of radical fragment yield as a function of E/N, and determination of scaling parameters.

Experimental Details

A schematic diagram of the experimental apparatus is shown in Figure 15. The main components of the apparatus are the discharge cell, the light detection electronics, and the high voltage pulser. The discharge cell was a cylindrical glass enclosure, approximately 37 cm in height and 7.5 cm in diameter. Two sets of opposed fused silica windows (5-cm diameter), orthogonal to each other, were available as viewports. The cell was evacuated through 3.5-cm i.d. glass and metal lines by a roughing pump. The base pressure for the cell was 3 mTorr.

The discharge gas flow was metered by flow controllers (MKS Type 1259 flow controller and a MKS Type 247C four-channel readout), while the cell-pressure was governed by a control valve and an exhaust valve controller (MKS Types 253A and 252, respectively). The gas pressure was measured with a baratron pressure gauge (MKS Type 102A) whose output was sent to the valve controller to maintain constant pressure in the discharge cell. The gas flow could be varied between 0 and 100 SCCM, and the baratron operated in the pressure range 0-100 Torr. Gas pressure and flow rate were set by input to the PC. Throughout this study the gas flow rate was fixed at 30 SCCM and the pressure (p) at 50 Torr. Discharge gases were UHP grade (99.999%).

The discharge electrodes were two aluminum discs, 3.2 cm in diameter with an interelectrode spacing (d) that varied between 0.25 - 1.0 cm in this work (pd range 12.5 - 50 Torr cm). The discharge pulse repetition rate used was 10 Hz throughout. The interelectrode space could be illuminated by an UV preioniaztion lamp. The high voltage pulser constructed for this study powered the discharge and is based upon a stacked MOSFET switch. Output current/voltage measurements were made using high voltage probes (HP Model P6015) across the discharge and across a series current sense resistor. The probe outputs were monitored by a digital oscilloscope (LeCroy 9354C) for signal capture and averaging (100 shots). Current and voltage waveforms were then transferred to a PC for processing.

High speed direct discharge imaging and spectral imaging were done using a gateable, intensified CCD camera (Princeton Instruments Model ICCD-576). Spectral images were made using 10-nm bandpass filters at 431 nm (CH) and 516 nm (C_2). Time resolved H , CH or C_2 emissions from the discharge were detected using a gated

photomultiplier tube (PMT, Hamamatsu R1477). Light was collected through an iris diaphragm by a focusing lens and passed through the various bandpass filters onto the PMT. The PMT was under a constant bias throughout the experiment, and was gated on for a 5- s period encompassing the discharge pulse duration. Neutral density filters were used to avoid saturation. The PMT output was amplified and sent to a digital oscilloscope for signal capture and averaging (100 shots), and to a PC as above. Single-shot C_2 emission profiles were also recorded. When discharge imaging is not being conducted, a second gated PMT in place of the camera allows for simultaneous time resolved emission spectroscopy of a pair of methane fragments.

Results

Discharge Characterization

Averaged current, gap voltage and power waveforms for discharges in pure methane (flows) at 50 Torr and using a 5 kV pulser drive voltage are shown in Figure 16 for four different electrode spacings (1.0, 0.75, 0.50 and 0.25 cm). The pulser provides rapid excitation pulse rise and fall times (typically < 20 ns), control over pulse duration, and low jitter (typically < 10 ns). Note that the discharge current turns on earlier as the gap is decreased. A fixed trigger pulse width of 440 ns was used throughout this work. (and the discharge pulse width variation results from that turn-on trend.)

The current pulse rise is typically delayed relative to that of the gap voltage pulse by roughly 25 ns in each case, and there is a substantial overlap between current and voltage during the short initial peak in the voltage pulse. The power curves reflect the degree of overlap with the brief (~30 ns FWHM), high-power initial peak that occurs at each gap. Additionally, no indications of arc formation are seen by way of sudden voltage drops and associated current excursions; pulse-to-pulse shape variations are minimal.

In all cases the gap voltage falls to a lower steady state value after the initial peak until the pulser is triggered off. This implies that discharge E/N is substantially higher during the initial pulse peak than in the relatively long final steady state period. In order to determine E/N from the gap voltage and the discharge conditions (50 Torr, 300 K), the voltage drop across the thin (~ 50 m) cathode sheath must subtracted. The sheath drop and average E/N for the discharges were estimated during the steady state portion by plotting the average voltage (between 200 - 400 ns) against electrode separation, as shown in Figure 17. Though pd varies by a factor of 4, the data bear the usual linear relationship[17, 18], and indicates reasonable values for both the sheath drop of 300 V, and an average E/N of 80 Td. When that sheath voltage drop is subtracted from the measured gap voltages, shown in Figure 16, average E/N during the steady state portion of the discharges agrees well with that value. E/N conditions during the initial breakdown portion of the discharge pulses range up to a factor of four higher than the steady state portion of the pulse.

The range of E/N values found here is attractive from the viewpoint of assessing the hydrocarbon fragment yield as a function of E/N. To determine if the discharge can also be made sufficiently diffuse to facilitate fragment yield measurements by laser spectroscopy techniques, discharge imaging, spectral imaging, and time-resolved spectroscopy techniques were used. Due to the short duration of a typical discharge pulse, the discharges were imaged with a gateable, intensified CCD camera to determine the degree of homogeneity and pulse-to-pulse variability.

Discharge V-I pulse shapes, especially risetimes, and discharge pd values, are important determinants of discharge uniformity[17, 18], as are levels and methods of discharge gas preionization[19]. Using discharge conditions identical to those shown in Figures 16 and 17, Figure 18 shows typical 100 ns exposures documenting the (dramatic) effect that decreasing the electrode spacing has upon discharge uniformity. The transition between multiple streamer discharge and diffuse discharge occurs under the indicated conditions between 0.5 cm and 0.25 cm gaps, or below a pressure-discharge gap product (pd) of 25 Torr-cm. (All discharge gaps studied show sufficient homogeneity to allow for the application of laser spectroscopy techniques.)

The behavior of the discharge as a function of pulser drive voltage is shown in Figure 19 for a fixed gap of 1.0 cm and drive voltages of 4, 6 and 8 kV. All other experimental parameters are identical to those discussed above. Features here are similar to those of Figure 16, except that the current risetime and turn on time are much slower for the lowest drive voltage. Here too the gap voltage pulses peak just before the corresponding current turns on, the degree of overlap being reflected in the corresponding power curves. The overvoltage at the beginning of the pulse is clearly most effective for power deposition at high E/N conditions.

Extracting the temporal evolution of discharge E/N from the above gap voltage pulses was accomplished by subtracting a scaled sheath voltage drop from the gap voltage and accounting for discharge conditions (300 K, 50 Torr, 1 cm gap). The result is shown in Figure 20. Again note the overlap with the corresponding current pulses: the high E/N values early-on for the 4 kV drive voltage is largely ineffective given the late turn on time for that case. However, the high peak power for the higher drive voltages substantially overlaps the early high E/N values, a result that is a major determinant of time resolved hydrocarbon fragment emission profiles.

Time resolved H and CH band emissions (431 nm) for experimental conditions identical to those shown in the previous two figures are shown in Figure 21. The effect on direct electron impact excited methane fragment (H(n=3) and CH(A^2 . states) production of the early high E/N values for the higher drive voltages is clear, though the emission profiles and relative intensities are somewhat different. Both emissions rise at the same rate as the discharge power pulse indicating direct electron impact dissociative excitation of methane as their sources. The brighter (factor of five) CH emission has a markedly long fall time due to the long radiative lifetime and the low quenching[20] rate compared to very strongly quenched[21, 22] H(n=3) atomic level. At 50 Torr the H emission profile very closely resembles that of the discharge power for all drive voltages.

For the higher drive voltages there is a short current peak at the beginning of the pulses. However, both the H and CH emissions are much more significantly enhanced at the beginning of the pulse than current pulse shapes would suggest, thus showing the effect on methane fragmentation which results from the high E/N conditions at the early on.

The final time resolved emission results from CH_4 discharges reported here are for the C_2 Swan bands[12, 13] near 516 nm. Complemented by (direct) discharge imaging and spectral imaging of the C_2 and CH bands, the rare occurrence of highly inhomogeneous discharges can be partially understood. On rare occasions (direct) discharge images indicated the presence of only one or two very bright streamers in the discharge. Almost entirely absent at the smallest gap studied, the incidence of such highly inhomogeneous discharge pulses grew to roughly 3 percent of pulses at the largest gap of 1.0 cm. Further, a dramatic increase in bright streamer formation frequency occurred in the absence of irradiation of the discharge space by the UV preionization source. Insights into a potential cause of the formation of a few bright streamers as opposed to multiple streamer discharges were suggested by related on-going investigations[23]. Vibrationally hot C_2 bands have been observed in similar discharges, and at higher pressures (100 Torr) visible carbon deposits have been observed to form on the discharge electrodes.

Figure 22 shows five single-shot current pulses and their corresponding C_2 (A^3 $_g$ – X^3 $_u$, v = 0) emission profiles (near 516 nm), taken with and without UV preionization of the discharge (gas). (Direct) Images of those same pulses are shown in Figure 23. The discharge conditions were 0.75 cm discharge gap, 50 Torr methane, and drive voltage of 5 kV. Except for a delayed single shot in the case without UV irradiation, the current pulses are essentially identical between the two cases, and clearly quite repeatable. The clearest difference between the two data sets is the much greater brightness without UV irradiation. Inspection of Figure 23 correlates the bright streamer discharge conditions with bright C_2 emission. The rise of the more typical diffuse, weak emissions in the case with UV irradiation essentially follows the current. (This suggests excitation by direct electron impact, requiring the carbon molecules to be normal, low density gap constituents.)

Clearly, the discharge fully dissociates some fraction of methane, and some carbon atoms subsequently combine to form C_2 and presumably larger carbon clusters. The rise in the bright carbon emissions associated with bright streamer appearance is longer and slower to steady state, after an initial rapid rise similar to the weak emissions case. The brighter emission and different temporal emission profile suggest the possible involvement of large carbon clusters breaking up under direct electron impact within the gap, or being detached from the cathode and breaking up as the pulse rises. Carbon clusters that formed during repetitive pulsing of the discharge could adhere to the electrodes providing both the source of the bright streamers as well as the vibrationally hot C_2 bands.[23] Such processes would locally enhance the discharge conductivity and contribute to the formation of inhomogeneous plasmas with one or two bright streamers. The C_2 emission profiles in the case of highly inhomogeneous bright

streamer discharges are different from any other observed emission profile (see Figure 21), suggesting different kinetics involved in excitation of the C_2 molecule in those cases.

The final experimental results associated with the discharge characterization show the spatial distribution of C_2 emissions in comparison with that of the brightest hydrocarbon fragment emission bands of CH. Figure 24 shows images of the discharges similar to those of Figure 23, except that they have been imaged through bandpass (10 nm FWHM) filters. The typical spatial distribution of the C_2 emission is quite uniform and weak (upper left) when the discharge is diffuse, indicating a largely uniform distribution of C_2. Bright streamer formation is clearly accompanied by strongly enhanced C_2 emission (upper right). The spatial distribution of the CH emission is quite similar to that of C_2 regardless of the degree of discharge homogeneity.

H-atom Production

Using the technique of actinometry[24-27], an estimate of H-atom production during a discharge pulse can be made by comparing the H emission from the methane discharge (Figure 21) to that from the very well characterized pure H_2 discharge[1, 2, 14-16] under the same experimental conditions. Gap voltage, discharge power, and the resulting H emission from discharges into pure hydrogen at 50 Torr using a 6 kV pulser drive voltage are shown in Figure 25. The temporal behavior of the gap voltage and discharge power are very similar to the analogous case for discharges into methane (see Figure 19, 6 kV drive voltage case), although both fall more rapidly in the hydrogen plasma during the latter portion of the discharge pulse. This behavior clearly indicates that discharge E/N in the pure hydrogen discharges decreases somewhat more during the latter portion of the discharge pulse, as opposed to remaining essentially constant after the initial high E/N peak in methane (see Figure 20, 6 kV case). The likely cause of the minor difference in temporal behavior is that the methane plasmas are slightly electronegative. The H emission from the pure hydrogen discharge shown in Figure 25 follows the discharge power pulse, identical to the temporal behavior of the H emission from methane (compare to Figure 21, 6 kV case).

Discharges in pure hydrogen have been extensively studied[1,2,14-16], and the fraction of the discharge power deposited into the various inelastic modes of hydrogen as a function of E/N has been established. For E/N above 80 Td the fraction of the discharge power producing dissociation[2] of H_2 into two H atoms is greater than 50 %. Absolute H atom density and H emission measurements[1] for such discharges have also made as a function of discharge E/N. Thus, it is possible to write the number density of H atoms in pure hydrogen discharges as,

$$[H]_{H2} = \frac{2\int X(E/N)\, P_{H2} dt}{D_e\, V}, \qquad (1)$$

where P_{H2} is discharge power, $X(E/N)$ is the known fractional power deposition into dissociation[2] as a function of E/N, D_e is the dissociation energy of H_2 (9.8 eV), and V is

the discharge volume. The factor of 2 accounts for the fact that each dissociation event produces two hydrogen atoms. Equation (1) can be used to directly determine the H-atom production in pure hydrogen discharges from electrical measurements alone.

H emission from such a discharge results from the competition between production of H(n=3) atoms, and losses by radiation, or by collisional quenching, to the ground state. As noted above, the rapid rise of H emission (in concert with the rise in the discharge power pulse) indicates that production of H(n=3) atoms in this study proceeds by direct electron impact dissociative excitation of the parent gas. The resulting H emission intensity can be written[24-27] as the ratio of the rate of production to that of loss:

$$I_{H\alpha}^{H2} = \frac{Ch\nu_{32}A_{32}k_e^{H2}n_e^{H2}[H_2]}{\sum_j A_{3j} + k_Q^{H2}[H_2]}. \qquad (2)$$

Here n_e^{H2} is the electron density in the hydrogen discharge, h_{32} and A_{32} are the photon energy and Einstein coefficient for spontaneous emission for the transition, respectively, A_{ij} is the sum of the A coefficients for all radiative de-excitation processes from the H(n=3) level (H and Lyman), and C is a constant that contains all optical and geometrical parameters such as solid angle viewed, transmissions, and detection system response. The coefficients k_e^{H2} and k_Q^{H2} quantify electron impact dissociative excitation of H_2 to H(n=3) + H(1s) and the quenching rate of H(n=3) atoms in hydrogen, respectively. The square brackets denote concentration.

For discharges into pure CH_4, the resulting H emission intensity can similarly be written as,

$$I_{H\alpha}^{CH4} = \frac{Ch\nu_{32}A_{32}k_e^{CH4}n_e^{CH4}[CH_4]}{\sum_j A_{3j} + k_Q^{CH4}[CH_4]}, \qquad (3)$$

where the symbols have analogous meanings. The ratio of H emissions from the two discharges then is simply,

$$\frac{I_{H\alpha}^{H2}}{I_{H\alpha}^{CH4}} = \frac{k_e^{H2}n_e^{H2}[H_2]}{k_e^{CH4}n_e^{CH4}[CH_4]} \frac{\sum_j A_{3j} + k_Q^{CH4}[CH_4]}{\sum_j A_{3j} + k_Q^{H2}[H_2]}. \qquad (4)$$

It has been shown that H-atom production in (fast) pulsed discharges in hydrogen (measured by two photon allowed laser induced fluorescence or TALIF) is directly proportional to the H emission signal[1]. The same relation between H-atom production and H emission should hold for discharges in methane since the thresholds for both electron impact dissociative excitation[28,29] (DE) and dissociation[30,31] (D) are nearly the same in both hydrogen and methane, i.e.

$$(E_{th}^{H2}(DE) = 19\ eV,\ E_{th}^{CH4}(DE) = 20\ eV,\ and\ E_{th}^{H2}(D) = 9.8eV, E_{th}^{CH4}(D) = 8.8eV).$$

The threshold for direct electron impact excitation of H atoms to H(n=3) is, of course, independent of the parent gas. Together, these facts allow replacement of the

ratio of production rates of H(n=3) atoms by dissociative excitation in Equation (4) with the corresponding rates of direct electron impact excitation of ground state H atoms to the H(n=3) level. With that substitution Equation 4 becomes,

$$\frac{I_{H\alpha}^{H2}}{I_{H\alpha}^{CH4}} = \frac{k_{ei}^{H2} n_e^{H2} [H]_{H2}}{k_{ei}^{CH4} n_e^{CH4} [H]_{CH4}} \frac{\sum_j A_{3j} + k_Q^{CH4}[CH_4]}{\sum_j A_{3j} + k_Q^{H2}[H_2]}, \qquad (5)$$

where the subscript *ei* indicates the rate coefficient for electron impact of H atoms to H(n=3), and $[H]_{H2}$ and $[H]_{CH4}$ refer to the concentration of H atoms in the hydrogen and methane discharges, respectively.

The product of the direct electron impact excitation rate coefficient and electron density in the each plasma is proportional to the fraction of discharge power devoted to that process multiplied by the power deposited in the gas, i.e.:

$$k_{ei}^{H2} n_e^{H2} \propto Y(E/N)\, P_{H2}, \text{ and } k_{ei}^{CH4} n_e^{CH4} \propto Y'(E/N)\, P_{CH4}, \qquad (6)$$

where $Y(E/N)$ is the known[2] fractional power deposited into electron impact production of H(n=3) as a function of E/N in hydrogen, and $Y'(E/N)$ is the analogous factor in methane discharges. Note that the proportionality constants in Equations (6) are the inverse of the excitation potential of H(n=3), and are therefore identical for each of those relations. Substitution of Equations (1) and (6) into Equation (5), and ***assuming*** $Y \approx Y'$, the final expression used to estimate H atom production in the CH_4 discharges of interest can be written as,

$$[H]_{CH4} \approx \frac{I_{H\alpha}^{CH4}}{I_{H\alpha}^{H2}} \frac{P_{H2}}{P_{CH4}} \frac{\sum_j A_{3j} + k_Q^{CH4}[CH_4]}{\sum_j A_{3j} + k_Q^{H}[H_2]} \frac{2\int X(E/N)\, P_{H2} dt}{D_e V}. \qquad (7)$$

In this relation, the relevant quenching rate constants for H(n=3) atoms[21,22] are 2 x 10^{-9} cm^3/s in H_2 and 3.5 x 10^{-9} cm^3/s in CH_4, and the measured H intensity profiles needed as inputs are shown in Figures 21 (6 kV drive voltage case) and 25 for emission from methane and hydrogen discharges, respectively. The discharge power profiles are shown in Figure 19 for methane (6 kV drive voltage case) and Figure 25 for hydrogen. The factor *X* was taken to be 0.6 during the initial high E/N peak in the power pulse, and 0.45 during the much longer steady state portion of the discharge (see Figures 20 and 25).

Using Equation (1), the H-atom production during a single discharge pulse into 50 Torr of pure hydrogen using a pulser drive voltage of 6 kV was calculated and is shown as the upper plot in Figure 26. Similarly, using Equation (7), the H-atom production during a single discharge pulse into methane under the same experimental conditions is shown in the lower plot of that figure. For comparison purposes, the discharge pulse power and the associated emission are also shown in that plot. Note that the production rate is significantly higher during the brief high E/N early peak in the discharge pulse that is typical in such fast discharges. Production of ≈3 x 10^{14} H atoms per cubic centimeter of discharge volume during a 400 ns discharge pulse is significant.

The total energy deposited in the gas during a pulse is 5.6 mJ, and the energy deposited per unit volume is 0.7 mJ/cm^3. Verification of that level of H-atom production will require the use of (more elaborate) two-photon laser induced fluorescence or mass spectrometric measurements CH_4 fragments.

Discussion and Conclusions

Techniques for the control of the transition from diffuse to inhomogeneous plasmas in high E/N hydrocarbon discharges have been established. (Plasma homogeneity can be made sufficient good to allow for further quantitative study of the hydrocarbon fragment yield by laser spectroscopic techniques). The steady state portion of the discharge voltage pulse follows the classic pd scaling[17,18] relationship over the pd range studied (12.5 - 50 Torr cm). The resulting plasmas are typically diffuse in the lower end of that pd range, and even at the higher pd values are sufficiently uniform (multiple streamers). (for laser diagnostic techniques to be applied.)

The association of bright C_2 emission with the most inhomogeneous discharge plasmas, and the strong inhibiting influence that discharge gas preionization has over their formation, are clearly established. The possible role of carbon clusters in the formation of plasma inhomogeneities should be studied further. A potentially attractive method for carbon concentration modification in the discharges could be the addition of N_2. Any eventual scramjet ignition system would have to allow for the presence of atmospheric nitrogen, and the formation of CN radicals should result in a reduction in the carbon concentration and attendant cluster formation. CN formation (should) can be easily monitored by optical spectroscopy.

Significant levels of hydrogen atom production by fast, high E/N discharges are estimated from the measured H emission profiles and by the application of an actinometric model. The results are quite encouraging from the viewpoint of application to scramjet ignition and combustion sustainment. (Verification of that estimate will require much more elaborate experimental investigations.)

References:

1. J.M. Williamson and B.N. Ganguly, Phys. Rev. E **61**, 5734 (2000).
2. R. Nagpal, B.N. Ganguly, P. Bletzinger and A. Garscadden, Chem. Phys. Lett. **257**, 386 (1996).
3. T.C. Wagner, W.F. O'Brien, G.B. Northam and J.M. Eggers, J. Propulsion **5**, 548 (1989).
4. T. Mitani, Combust. Flame **101**, 347 (1995).
5. K. Khodataev and A. Ershov, in *2nd Weakly Ionized Gases Workshop, Proceedings Supplement*, Norfolk, VA, p. 341-350, (1998).
6. Y.Y. Buriko, V.A. Vinogradov, V.F. Goltsev and P.J. Waltrup, J. Prop. Pwr. **18**, 1049 (2002).
7. S.L. Yao, E. Suzuki and A. Nakayama, Plasma Chem. Plasma Proc. **21**, 651 (2001).
8. S.L. Yao, E. Suzuki, N. Meng and A. Nakayama, Plasma Chem. Plasma Proc. **22**, 225 (2002).
9. K.-T. Rie, E. Menthe and J. Wohle, Surf. Coat. Tech. **98**, 1192 (1998).
10. W.W. Stoffels, E. Stoffels, G. Ceccone and F. Rossi, J. Vac. Sci. Technol. A **17**, 3385 (1999).
11. I. Geraud-Grenier, V. Massereau-Guilbaud and A. Plain, Eur. Phys. J. AP **14**, 187 (2001).
12. G. Herzberg, *Electronic Spectra of Polyatomic Molecules*, (Van Nostrand, Princeton, NJ, 1966).
13. R.W.B. Pearse and A.G. Gaydon, *The Identification of Molecular Spectra*, (Wiley, New York, 1976).
14. B.N. Ganguly and P. Bletzinger, J. Appl. Phys. **82**, 4772 (1997).
15. P. Bletzinger and B.N. Ganguly, Chem. Phys. Lett. **247**, 584 (1995).
16. B.N. Ganguly and P. Bletzinger, Appl. Phys. Lett. **72**, 1570 (1998).
17. A. Von Engel, *Ionized Gases, (*AIP, New York, 1995).
18. E. Nasser, *Fundamentals of Gaseous Ionization and Plasma Electronics*, (Wiley, New York, 1971)
19. T.A. Beer, J. Laimer, and H. Stori, H., J. Vac. Sci. Technol. A **18**, 423 (2000).
20. J.L. Cooper and J.C. Whitehead, J. Chem. Soc. Faraday Trans. **88**, 2323 (1992).
21. M. Glass-Maujean, S. Lauer, H. Liebel and H. Schmoranzer, J. Phys. B. **33**, 4593 (2000).
22. S. Lauer, H. Liebel, F. Vollweiler, O. Wilhelmi, R. Kneip, E. Fleming, H. Schmoranzer and M. Glass-Maujean, J. Phys. B. **31**, 3049 (1998).
23. Brown, M. and Ganguly, B., (private communication.) AIAA -2003-0702, 41st Aerospace Sciences Meeting and Exhibits, 6-9 January, Reno, NV
24. J.W. Coburn and M. Chen, J. Appl. Phys. **51**, 3134 (1980).
25. D. Pagnon, J. Amorim, J. Nahorny, M. Touzeau and M. Vialle, J. Phys. D. **28**, 1856 (1995).
26. H.C. Barashilia and V.D. Vankar, J. Appl. Phys. **80**, 3694 (1996)
27. H.M. Katsch, A. Tewes, E. Quandt, A. Goehlich, T. Kawetzki and H.F. Dobele, J. Appl. Phys. **88**, 6232 (2000).

28. R.K. Janev, W.D. Langer, K. Evans Jr. and D.E. Post Jr., *Elementary Processes in hydrogen-helium Plasmas*, (Springer, New York, 1989) p 20.
29. K. Motohashi, H. Soshi, M. Ukai and S. Tsurubuchi, Chem. Phys. **213**, 369 (1996).
30. R.K. Janev and D. Reiter, Phys. Plasmas **9**, 4071 (2002).
31. J. Bittner, K. Kohse-Hoinghaus, U. Meier, and T. Just, Chem. Phys. Lett. **6**, 571 (1998).

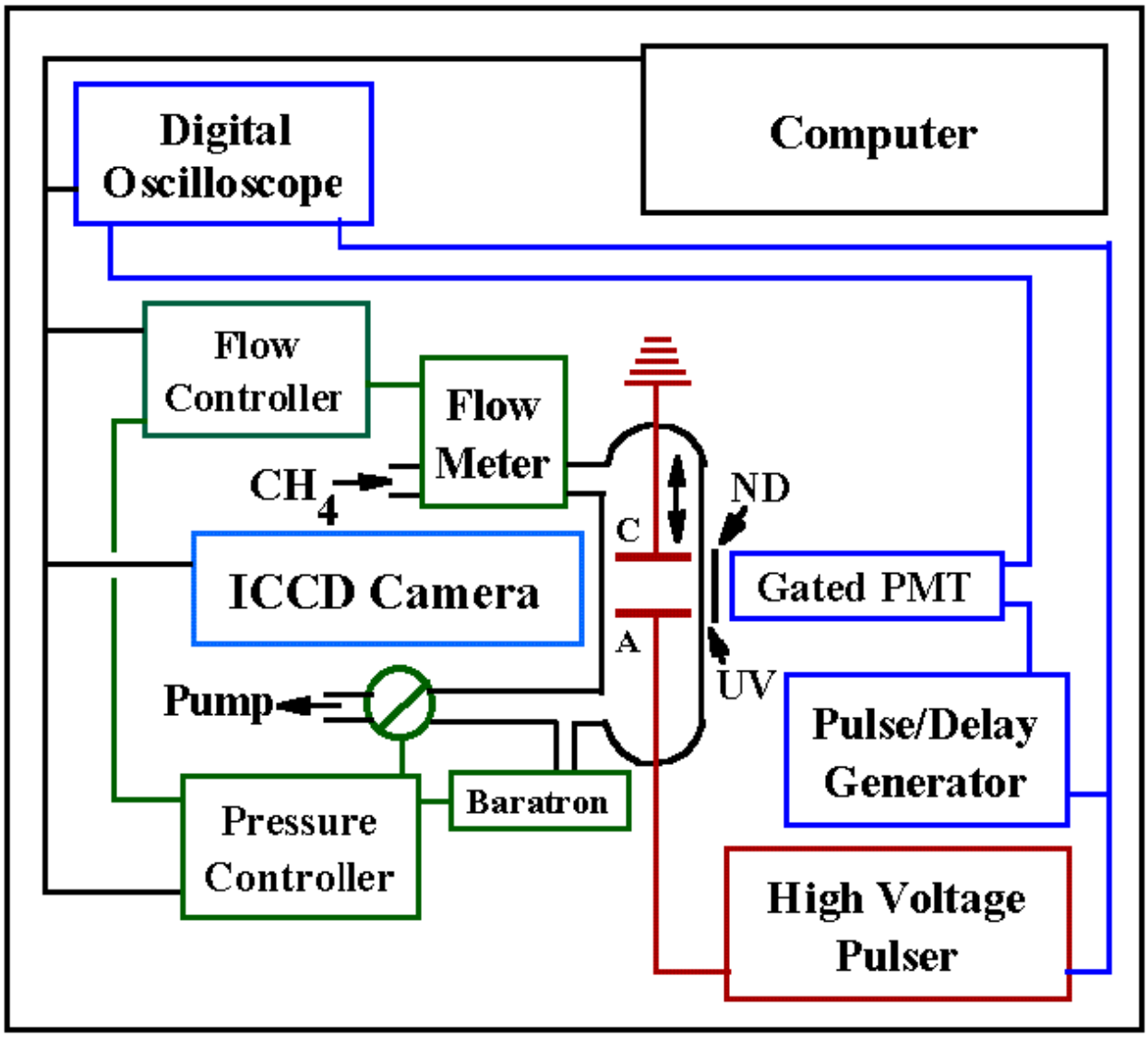

Figure 15. Schematic diagram of the experimental apparatus.

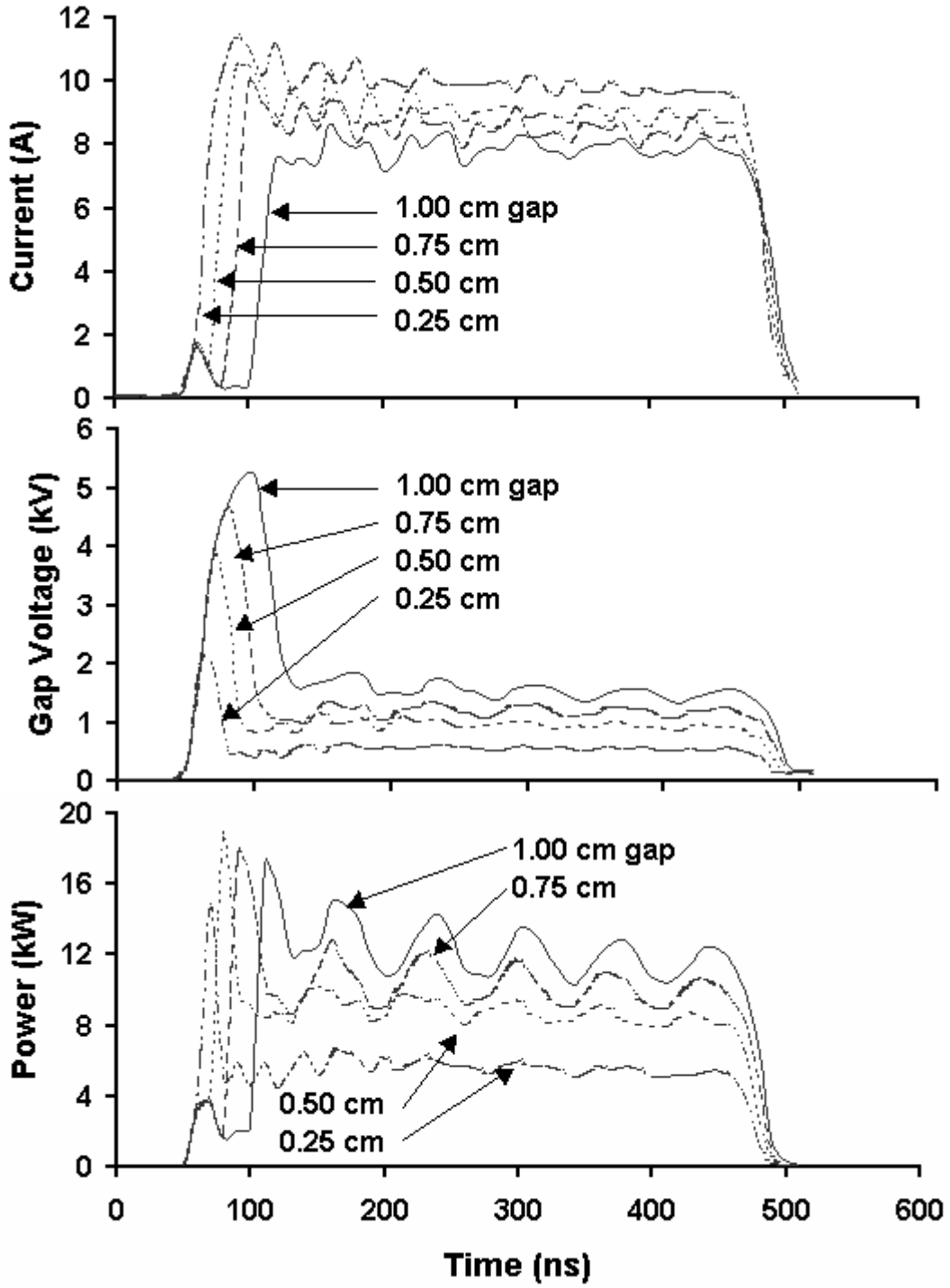

Figure 16. Current, gap voltage, and power characteristics for discharges into 50 Torr CH_4 and 5 kV pulser drive voltage as functions of discharge gap.

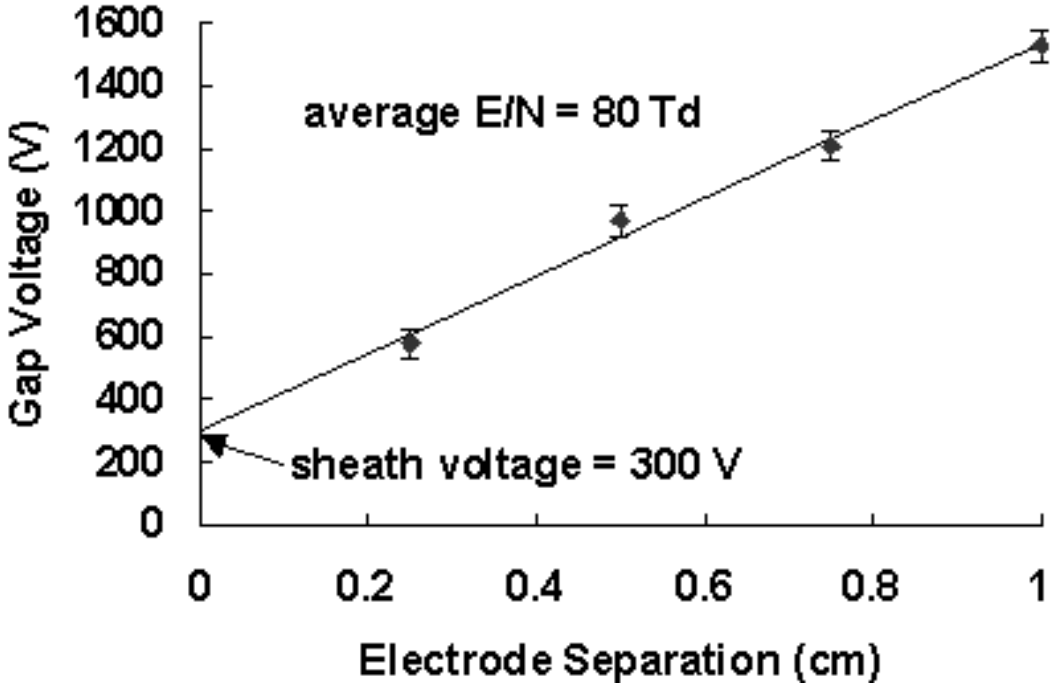

Figure 17. Average gap voltage between 200 - 400 ns plotted against anode-cathode gap (see Figure 16).

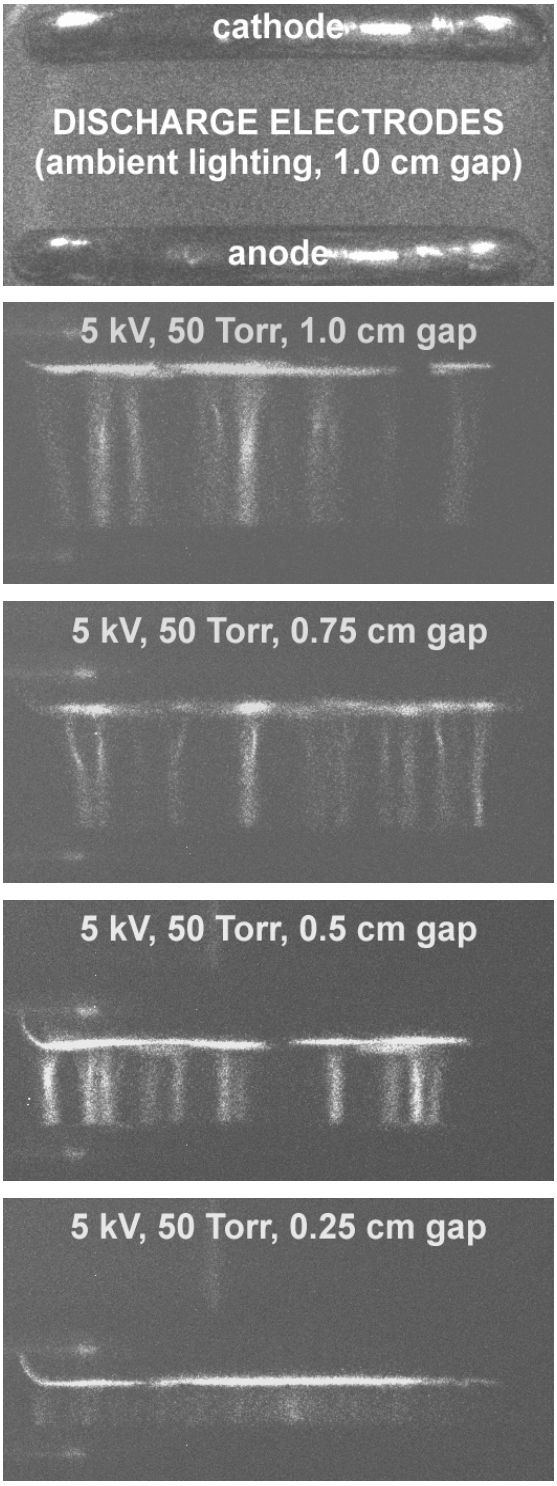

Figure 18. Direct, high-speed two-dimensional CH_4 discharge images as a function of interelectrode spacing.

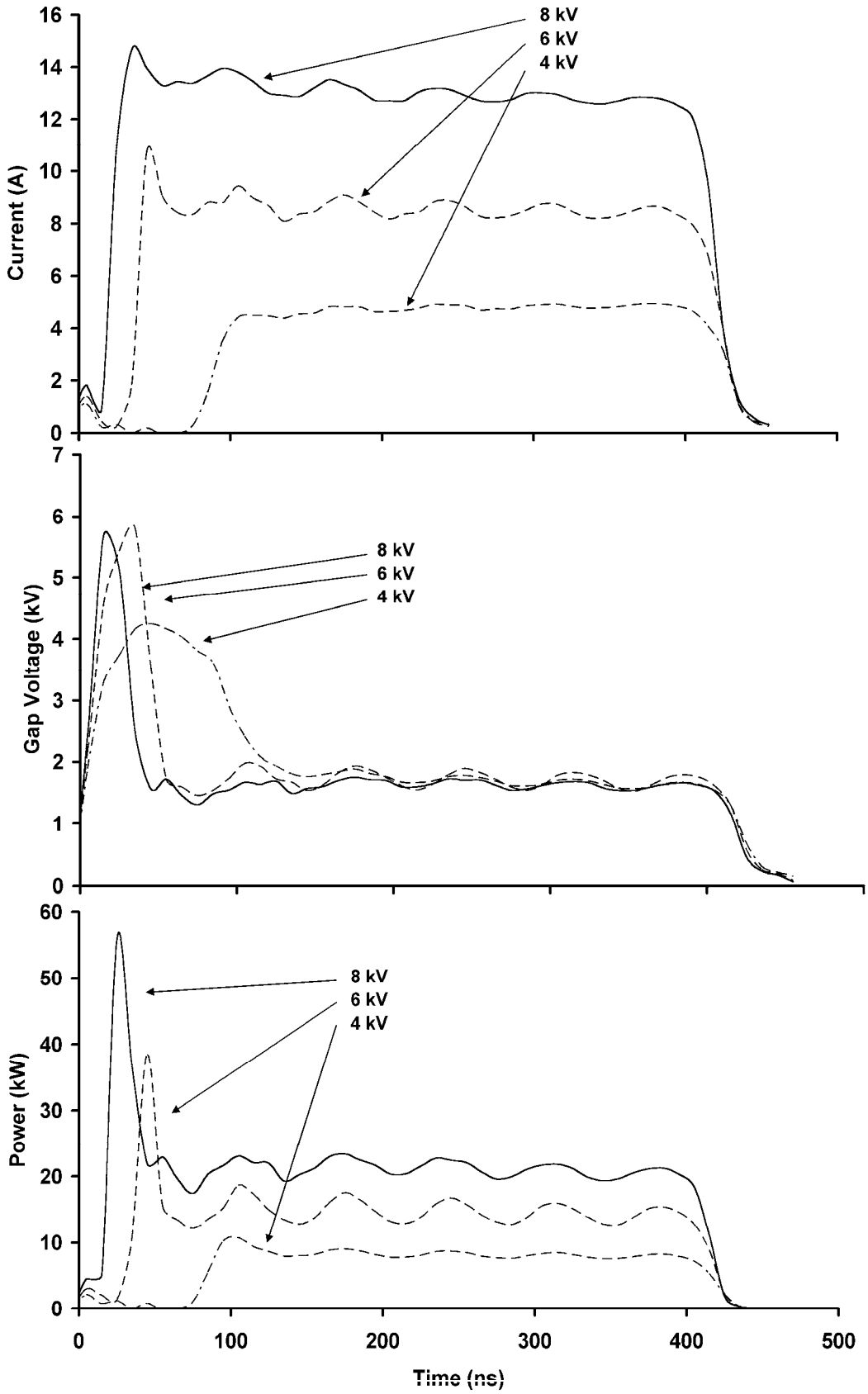

Figure 19. Current, gap voltage, and power characteristics as functions of pulser drive voltage for discharges into 50 Torr CH_4 and a 1.0 cm electrode gap.

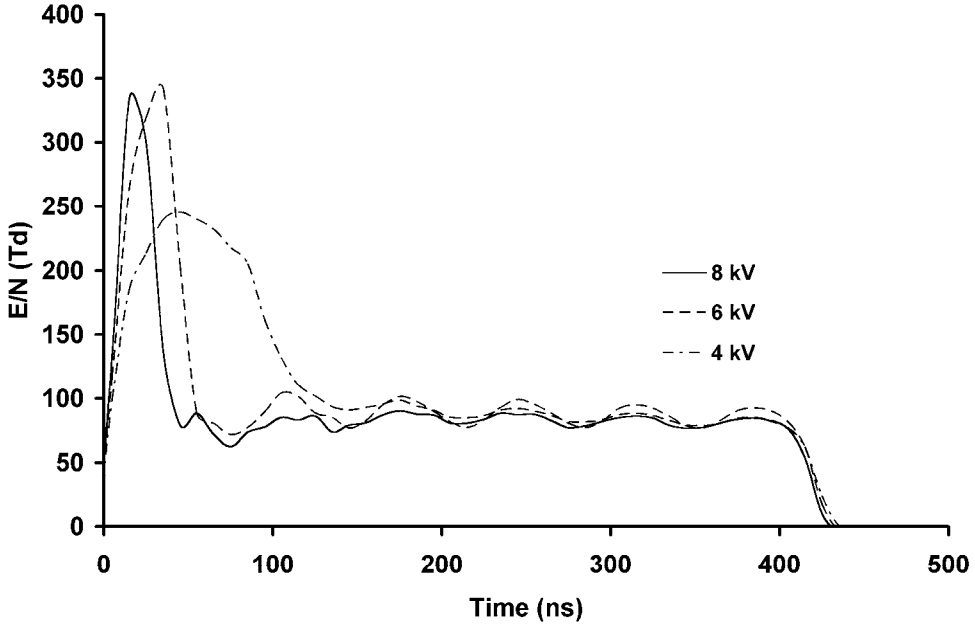

Figure 20. Temporal evolution of the discharge E/N for three drive voltages, a 1 cm gap, and 50 Torr methane.

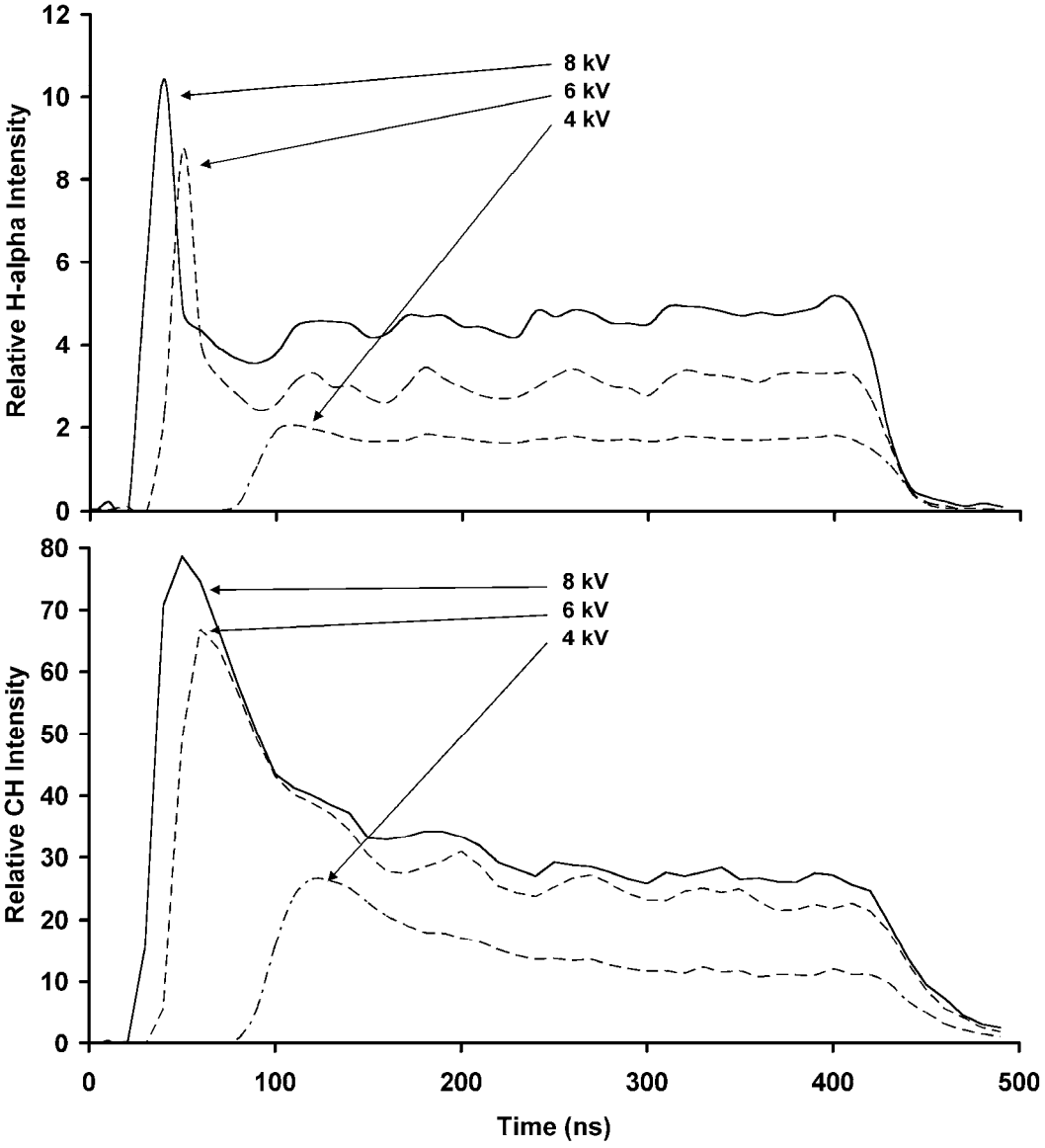

Figure 21. Temporal evolution of the most intense visible emissions from the excited hydrocarbon fragments: H and CH (431 nm band). Note that the H emission essentially follows the discharge power pulse while the CH emission peak occurs later in time. Experimental conditions are the same as for the previous two figures**.**

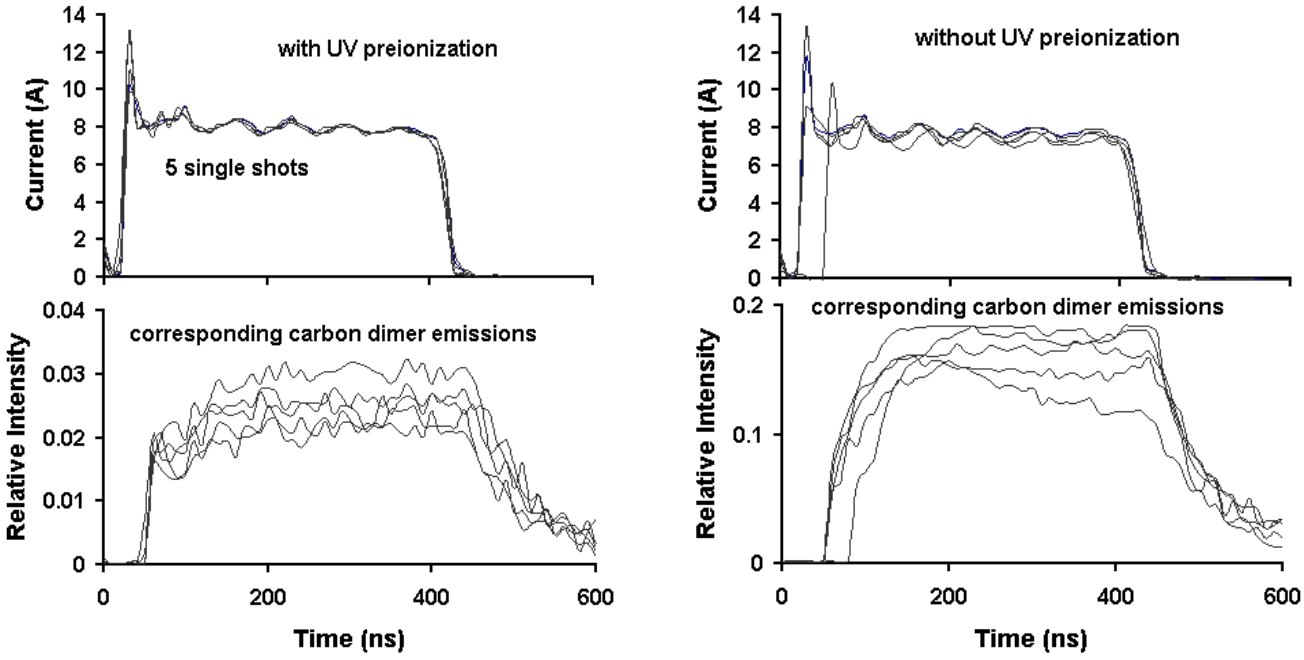

Figure 22. Single shot current pulses and the corresponding C_2 Swan band emission profiles near 516 nm for cases with and without UV irradiation of the discharge gas. Discharge conditions are 50 Torr methane, 5 kV drive voltage and fixed gap of 0.75 cm. The corresponding direct discharge images are presented in Figure 23.

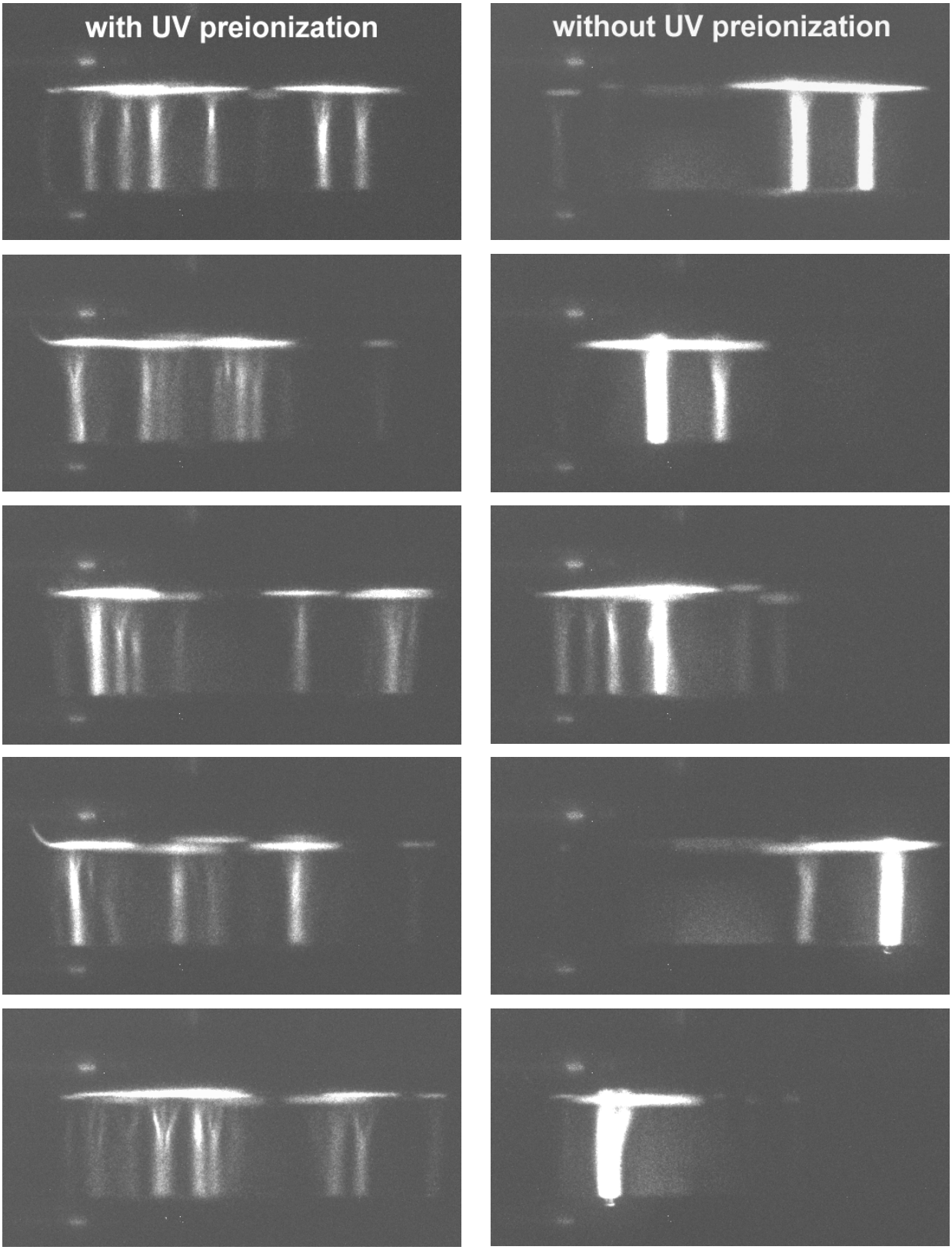

Figure 23. Direct discharge images of the same discharge pulses shown in Figure 24, with UV-irradiated discharges on the left. Bright streamer formation is much more common when the discharge gas is not preionized.

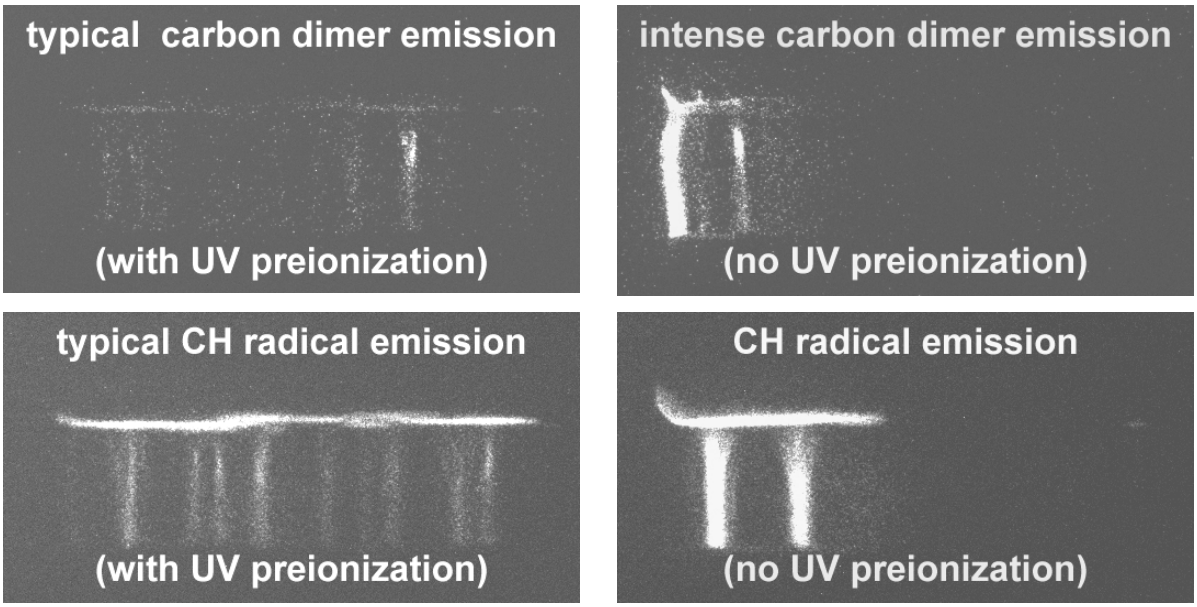

Figure 24. Spatial distribution of C_2 and CH emissions for typical discharges (left), and highly inhomogeneous bright streamer discharges (right).

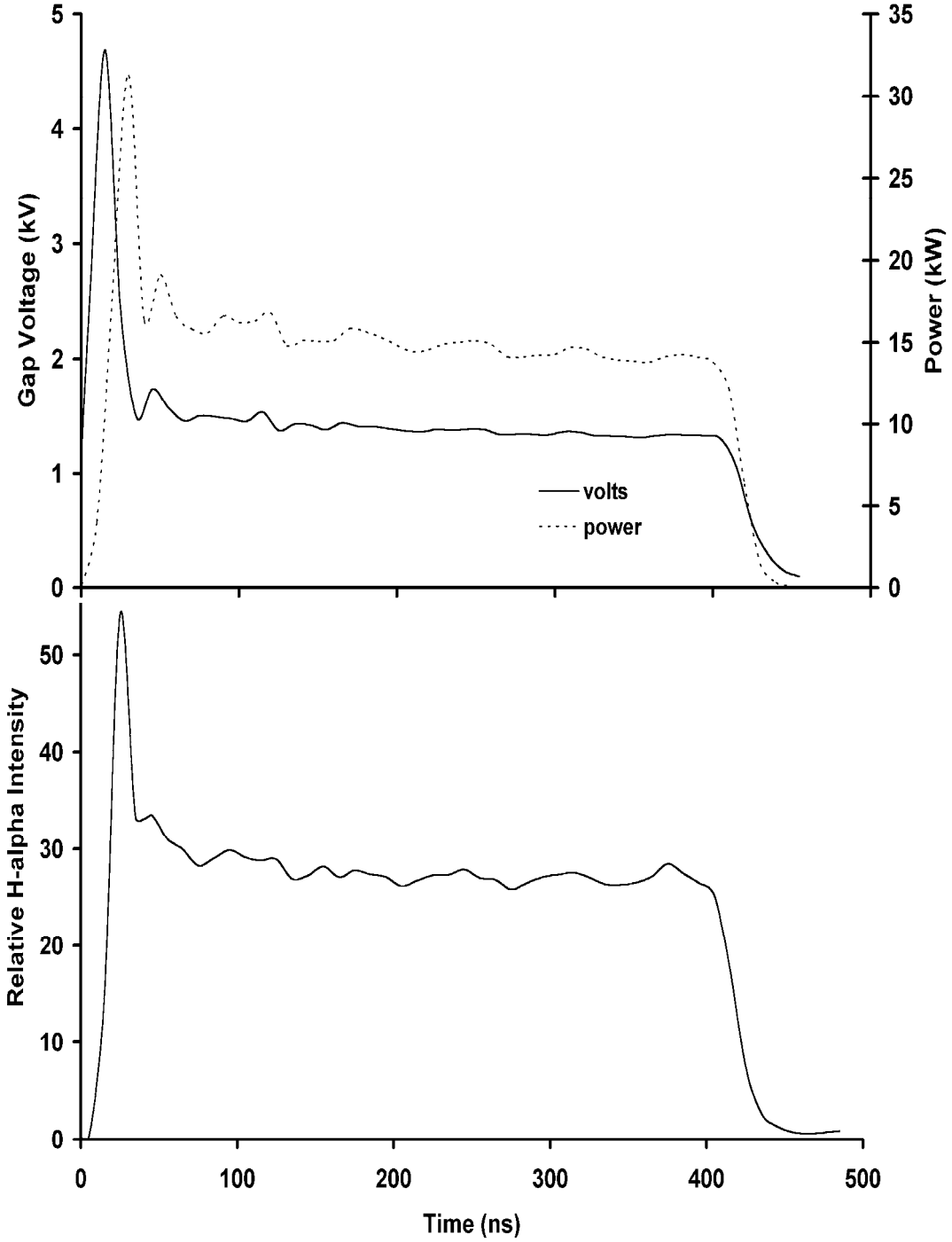

Figure 25. Current and gap voltage characteristics (top) and the resulting H_α emission (bottom) for discharges into pure H_2 at 50 Torr pressure, 1.0 cm gap, and a drive voltage of 6 kV (each area 100 shot averages. Compare to Figures 19 and 21 for CH_4 discharges.

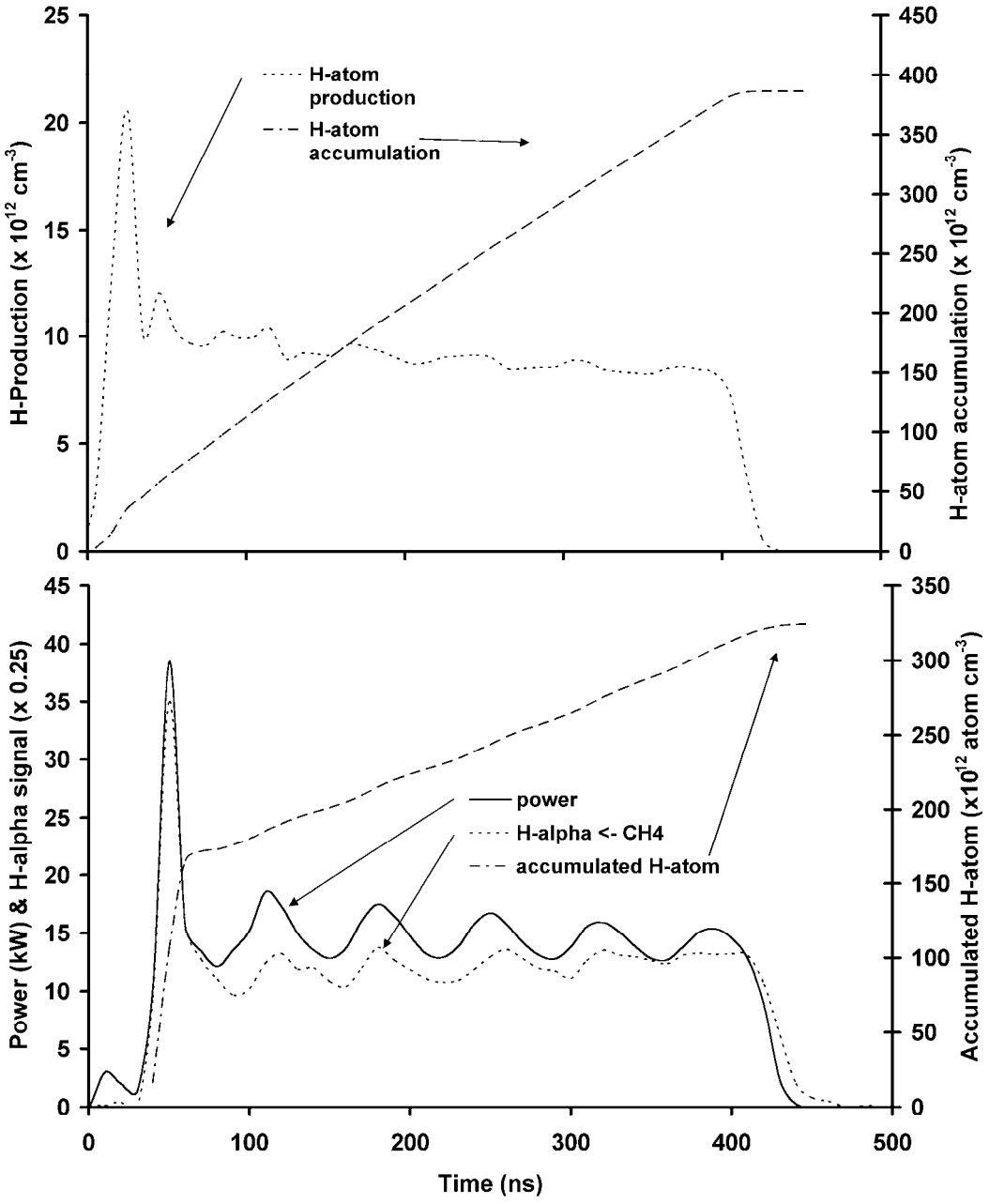

Figure 26. Estimated H-atom production in pure hydrogen (top) and methane (bottom), each during a discharge pulse. Both are determined from experiments using a 1 cm gap, a pulser drive voltage of 6 kV, and 50 Torr gas pressure.

VII. Appendix

Journal Publications/ Invited Presentations:

J. M. Williamson, P. Bletzinger, and B. N. Ganguly, "Gas temperature determination in a N2/Ar dielectric barrier discharge by diode-laser absorption spectroscopy and resolved plasma emission", J. Phys. D: Appl. Phys. **37,** 1658 (2004).

B. N. Ganguly and J. W. Parish ,"Absolute H atom density measurement in pure methane pulsed discharge", Appl. Phys. Lett. 84, 4953 (2004).

S. D. Marcum, J. W. Parish and B. N. Ganguly, "Methane Dissociation in Pulsed DC Discharges at High E/N", J. Propulsion and Power 20, No 2 (2004).

B. Bletzinger, B. N. Ganguly, and A. Garscadden, "Strong double layer formation by shock waves in nonequilibrium plasmas", Phys. Rev. E 67, 047401 (2003).

S. Dogan, A. Teke, D. Huang, H. Horkoc, C. B. Roberts, J. Parish, B. Ganguly, M. Smoth, R. E. Myers, and S. E. Saddow, "4H-SiC photoconductive switching devices for use in high power applications", Appl. Phys. Lett.,82, 3107 (2003).

P. Bletginzer and B. N. Ganguly, "The effect of displacement current on fast-pulsed dielectric barrier discharge", J. Phys. D: Appl. Phys 36, 1550 (2003).

M. S. Brown, J. D. Scofield and B. N.Ganguly, "Emission, thermocouple, and electrical measurements in $SF_6/Ar/O_2$ etching discharges", J. Appl. Phys.94, 822 (2003).

M.S. Brown, B. N. Ganguly, and A. Garscadden, "Resonance enhanced deactivation of Ar 4p' State by atomic oxygen and its impact on actinometry", Plasma Sources Sci. Technol, 11, 190 (2002).

B.N. Ganguly, P. D. Haaland, P. Bletzinger, and A. Garscadden, "Two color Mie scattering from uncorrelated and correlated dusty plasma", IEEE Trans. Plasma Science, 30, 90 (2002)

M. V. Ottugen and B.N. Ganguly, "Laser heterodyne method for high-resolution gas density measurements", Appl. Optics 40, 3502 (2001)

J. M.Williamson and B.N. Ganguly, "He metastable density in a double layer formed by a diameter discontinuity in a positive column", Phys. Rev E 64, September (2001).

C.Q. Jiao, B. Ganguly, C. A. DeJoseph and A.Garscadden, "Comparison of electron impact ionization and ion chemistries of CF_3Br and CF_3I", Int. J. Mass Spectrom. 208,127 (2001).

J. S. Shang, B. Ganguly, R. Umstattd, J. Hayes, M. Arman, and P. Bletzinger, "Developing a facility for Magneto-Aerodynamic Experiments", Journal of Aircraft 37, 1065 (2000).

P. Bletzinger, B.N. Ganguly, and A. Garscadden, "Electric field and plasma emission responses in a low pressure positive column discharge exposed to a low Mach number shock wave", Phys. Plasmas 7, 4341 (2000).

J. M. Williamson and B. N. Ganguly, "Hydrogen Dissociation in a $H_2 - N_2$ Pulsed DC Glow Discharge", Phys. Rev. E 61, 5734 (2000)

B.N. Ganguly and D.A. Dolson, "Direct comparison of electric field measurement by fluorescence and optogalvanic Stark spectroscopies", Plasma Source Sci. Technol. 9**,** 437 (2000).

J. D. Scofield, B. N. Ganguly, and P.Bletzinger, "Investigation of dilute SF_6 discharges for application to SiC reactive ion etching", J. Vac. Sci. Technol. A18, 2175 (2000).

P. Bletzinger and B.N. Ganguly, "Local acoustic shock velocity and shock structure recovery measurements in glow discharges", Phys. Lett A 258, 342 (1999).

A. Garscadden, P. Bletzinger, and B. N. Ganguly, "Acoustic Shock Interaction in a Positive Column Plasma", AIAA Paper No. 99-4973, AIAA Hypersonics Conference, Norfolk VA, Nov. 1-5, 1999 (invited paper).

B.N. Ganguly, P. Bletzinger and A. Garscadden, "Plasma-shock interactions in a low pressure positive column", IEEE Int. Conf. on Plasma Science, Monterey, CA, June 20-24, 1999 (invited paper).

M. W. Millard, P.P. Yaney, B. N. Ganguly and C. A. DeJoseph "Diode laser absorption measurements of metastable helium in glow discharges", Plasma Sources Sciences Technol. 7, 239 (1998).

J. D. Scofield, P. Bletzinger and B. N. Ganguly, "Oxygen free dry etching of α-SiC using dilute SF_6: Ar in an asymmetric parallel plate rf discharge", Appl. Phys. Lett. 73, 76 (1998).

B. N. Ganguly and P. Bletzinger, "Fractional dissociation efficiency measurements of D_2 in a helical resonator D_2-N_2 gas mixture discharge", Appl. Phys. Lett. 72, 1571 (1998).

B. N. Ganguly, "Shock wave propagation in glow discharges", Gaseous Electronics Conference and International Conference on Reactive Plasmas, Maui, HI October 19-22, 1998 (invited paper).

B. N.Ganguly and P. Bletzinger, "Comparison of hydrogen atom density measurements in three types of discharges using H_2-N_2 gas mixtures", J. Appl. Phys. 82, 4772 (1997).

B. N. Ganguly and P. Bletzinger, "High flux atom source for plasma processing", AIAA Conference on Plasmadynamics and Lasers Conference, Atlanta, GA June 23-25, 1997 (invited paper).

R. Nagpal, B. N. Ganguly, P. Bletzinger and A. Garscadden “Power Deposition in H_2 and H_2-N_2 Glow Discharges”, , Chemical Physics Letters, 257, 386 (1996).

P. Haaland, A. Garscadden and B. N. Ganguly “Ionic and Neutral Growth of Dust in Plasmas”, Appl. Phys. Lett. 69, 904 (1996).

B. N. Ganguly and Alan Garscadden “Phase Resolved Two-Dimensional Emission Pattern of a Low Frequency Helium Discharge”, IEEE Transactions on Plasma Science, 24, 115 (1996).

P. Bletzinger and B. N. Ganguly “High Fractional Dissociation Efficiency in H_2 and H_2-N_2 Gas Mixtures in a Helical Resonator Discharge”, Chemical Physics Letters, 247, 584 (1995)

B.N. Ganguly and P. Bletzinger, "Effect of Plasma-Surface Interactions on the Radial Variation of H atom Density In a Hydrogen Radio Frequency Discharge", J. Appl. Phys. 76, 1476 (1994).

P. D. Haaland, A. Garscadden, B. Ganguly, S. Ibram and J. Williams, "On Form and Flow In Dusty Plasmas", Plasma Sources Sci. Technol. 3, 381 (1994).

A. Garscadden, B.N. Ganguly, P.D. Haaland and J. Williams, "Overview of Growth and Behavior of Clusters and Particles in Plasmas", Plasma Sources Sci. Technol. 3, 239 (1994).

B. N. Ganguly, A. Garscadden, J. Williams and P. D. Haaland, "Growth and Morphology of Carbon Grains," J. Vac. Sci. Technol. All, 1119 (1993).

B. L. Preppernau and B. N. Ganguly, "Time Resolved Electric Field Measurements In a 15KHz Helium Glow Discharge," Rev. of Sci. Inst., July (1993).

M. J. Wolf and B. N. Ganguly “Rydberg State Stark Spectroscopic Measurement of Electric Field Profile in a Propane-air Flame”, Combust. Flame 90, 284 (1992).

B. N. Ganguly and A. Garscadden “Electric Field and Doppler Emission Profile Measurements In an Obstructed Hydrogen Discharge”, J. Appl Phys, 70, 621(1991)

S. D. Marcum, J. L. Myers, M. Tackett and B. N. Ganguly, “The Effect of Radiative Cascade on Electron Excitation Temperature Measurements”, J. Appl. Phys, 69, 27, (1991).